UNIVERSIDAD CARLOS III DE MADRID

Assessment of Load Alleviation in Aircraft due to Structural Flexibility

Author: Álvaro Tanarro del Río

Tutor: Pablo Fajardo Peña

A thesis submitted in partial fulfilment for the
degree of Bachelor in Aerospace Engineering

in the
Bioengineering and Aerospace Engineering Department
Escuela Politécnica Superior

June 2016

UNIVERSIDAD CARLOS III DE MADRID

Abstract

Bioengineering and Aerospace Engineering Department
Escuela Politécnica Superior

Bachelor in Aerospace Engineering

Álvaro Tanarro del Río

An evaluation of the effect of structural flexibility in aircraft loads is presented. The assessment is performed for two flight conditions: cruise and vertical gust encounter. These conditions are determined by several parameters, some of them based on actual certification regulations. To determine the effect of structural flexibility an aeroelastic model is developed: aerodynamic loads are obtained by a 3D numerical panel method based on vortex ring and horseshoe elements developed with Matlab [25], and structural deformation caused by external loads in a flexible structure is computed with ANSYS FEM software [3]. The model analysed is designed based on its aeroelastic modal frequencies. Different configurations of the wing are evaluated to determine the most relevant parameters involved in load alleviation. With the aim of updating the FEM model, a scaled specimen and a proper GVT are defined to obtain the real modal frequencies of the structure in future works and to use the experimental setup for teaching purposes at the university.

Acknowledgements

Definitely, thank my father and mother for their relentless help, support and encouragement during all these years. They are the reason why I have achieved the goals I have proposed to myself. A special mention to my father, who cannot be present in my actual and future accomplishments but he will be a very important part in all of them.

I also would like to thank my thesis tutor, Dr. Pablo Fajardo Peña, for his extraordinary support and involvement in the completion of this thesis. As well, thank Dr. Oscar Flores Arias for his advice and help in the coding of the 3D numerical aerodynamic method.

Last but not least, thank all the friends who have joined me during the degree. They have made this experience great and I hope this friendship lasts forever.

Contents

List of Figures

List of Tables

Abbreviations

DoF	**D**egree **o**f **F**reedom
EAS	**E**quivalent **A**ir **S**peed
EASA	**E**uropean **A**viation **S**afety **A**gency
FEM	**F**inite **E**lement **M**ethod
FW	**F**uel **W**eight
GVT	**G**round **V**ibration **T**est
HTP	**H**orizontal **T**ail **P**lane
IATA	**I**nternational **A**ir **T**ransport **A**ssociation
MLW	**M**aximum **L**anding **W**eight
MTOW	**M**aximum **T**ake **O**ff **W**eight
MZFW	**M**aximum **Z**ero **F**uel **W**eight
ODE	**O**rdinary **D**ifferential **E**quation
OEW	**O**perating **E**mpty **W**eight
PDE	**P**artial **D**ifferential **E**quation
PL	**P**ay**L**oad
SL	**S**ea **L**evel
TAS	**T**rue **A**ir **S**peed
UAV	**U**nmanned **A**erial **V**ehicle
VTP	**V**ertical **T**ail **P**lane

Symbols

t	thickness	m
w	width	m
f	frequency	Hz (s^{-1})
E	Young's Modulus	Pa
G	Shear Modulus	Pa
A	Area	m^2
l	Length	m
I	Area moment of inertia	m^4
J	Polar moment of area	m^4
L	Lift	N
W	Weight	N
N_z	Load factor	-
ρ	density	kg/m^3
ω	angular frequency	$rads^{-1}$
γ	torsional constant	m^4
ν	Poisson's Ratio	-
Γ	Vortex Circulation Intensity	m^2/s

Chapter 1

Introduction

Aerospace industry, together with nuclear industry, is the most challenging discipline that requires engineering knowledge. The reason for this is the impact that a mistake would have in terms of lives. IATA has forecasted that around 3.8 billion people will fly in 2016 [18], that means that aerospace industry covers up more than half the worldwide population (7.4 billion). However, differing from car industry, if a failure on a aircraft takes place, the result would be catastrophic. This leads into very strict safety regulations, certification specifications (i.e. CS-25 [10]), and fail-save design.

All these reasons make that aerospace industry does not only work with high technology but also focuses in every aspect that might affect aircraft performance. Aeroelasticity is one of those aspects whose study is fundamental in the safe operation of an aircraft. Aeroelasticity is defined as the study of the interactions between inertial, aerodynamic and elastic forces that occur when an elastic body is exposed to a fluid flow [17]. Some aeroelastic phenomena have caused accidents in which several lives were lost. One example is the accident of the Lockheed Model L-188C on March 17, 1960 in which 63 people died due to flutter phenomenon. Flutter is an aeroelastic phenomenon in which structure's inertia and elastic characteristics interact producing a self-excited oscillation that absorbs energy from the flow, inducing to a divergent oscillation that may cause severe structural failure [15]. Another aeroelastic phenomena that can cause structural damage is divergence.

The importance of aeroelasticity resides in the frequent conditions in which this field becomes relevant, for example, weather conditions are extremely important in the occurrence of the phenomena described since turbulence and gusts usually induce oscillations in the aircraft that might end in severe structural failure. Nevertheless, the aim of this work is not to study such effects but to focus on the effect of structural flexibility on the loads that an aircraft might suffer. Structural flexibility itself is not a drawback but the change in aerodynamic forces due to the elastic deformation of the structure may have a detrimental effect on aircraft performance or structural reliability [4].

1.1 Literature Review

The relevance of structural flexibility on aircraft loads is sustained by the numerous works found in the literature that have studied this effect and how it could impact aircraft performance at different conditions.

Xie et al.[37] present a non-planar vortex lattice method and perform the analysis by coupling of structural FEM deformations and the aerodynamic method. The results obtained by using the FEM software and the method developed are contrasted with an experimental investigation of the static aeroelasticity at a wind tunnel. The main conclusions obtained state that the linear aeroelastic method does not represent accurately the experimental output, but the non-linear method developed in this paper might provide acceptable results.

Ting et al. [33] develop a static aeroelastic model and study the longitudinal trim of a flexible wing aircraft. As the previous paper, in this investigation the solution is achieved by a structural FEM model and a vortex-lattice solver for the aerodynamics of the aircraft. A comparison between flexible and rigid on trimmed cruise flight is carried out.

Jacob [21] presents an experimental study of rigid and flexible aircrafts that encounter a gust. The static aeroelasticity of these aircraft is analysed by means of a wind tunnel. The load factor for both aircrafts is compared and different methods are studied to prove its validity in determining indirectly the deformation of the wing.

Raghavan et al. [28] study the aeroelasticity of oblique wings. For that purpose, they assess the longitudinal trim conditions of the aircraft for a rigid wing and for a flexible wing. Then, the same approach is followed but implemented into a full aircraft model, performing again a comparison between rigid and flexible aircraft.

Schweiger et al.[30] present a work in which different aeroelastic concepts are introduced. By studying the effects of these concepts on aerodynamic, structural and FCS capabilities of aircraft it is intended to achieve benefitial effects from the flexibility of the surfaces.

The main common aspect between most of the papers that carry out a simulation of structural flexibility effect is the methodology used to solve the problem. These simulations include a vortex-lattice method to solve for the aerodynamic loads and the structural deformation is obtained by means of a FEM software. Hence, the methodology used to perform the desired assessment will be based on a vortex-lattice method and a FEM simulation of the displacements using ANSYS structural module. However, although some papers perform the aeroelastic coupling with a different software, in this thesis the fluid-structure coupling is performed by direct application of the deformations into the aerodynamic model.

1.2 Objectives

The main purpose of this study is to analyse the effect of structural flexibility on the aerodynamic loads over an aircraft structure. Nonetheless, to achieve the main purpose of the thesis, some intermediate objectives must be accomplished along the analysis. These objectives can be summarized in the following goals:

- **Design a structural equivalent model**

As first step of the analysis procedure, a structural model on which the study will be performed must be designed. The structural model is aimed for simplified structural analyses, consequently the model can be made of metallic plates and beams. Nevertheless, although the model does not have to be equal to the real aircraft, its structural characteristics must be equivalent so the analyses performed can be applied to a real structure. To achieve equivalence, an optimization process will be performed by means of a modal analysis to get similar modal frequencies in the model to those obtained from the references. As foundation of the model, the dimensions of the C-295 will be scaled to a 2 m. span aeroplane so that the proportions of the model do not differ from those of a real aircraft.

- **Study the effect of structural flexibility on aerodynamic loads in cruise and uniform gust conditions**

Once the model has been designed to have proportional dimensions and similar modal frequencies than a real aircraft, the analysis of the effect of structural flexibililty on loads can be performed. The analysis is carried out by coupling of the fluid-structure interaction in two different environments (cruise and uniform gust) and by the development of an adequate methodology that includes code development and mesh refinement, together with different comparisons between theoretical and simulation results.

- **Redesign the model for its use to obtain the experimental modes**

The last goal of the project is to design a feasible experimental specimen and procedure to be used in experimental modal analysis tests. In order to achieve this goal, the model must be scaled to smaller dimensions so it can be handled within the university installations. The scaling process is the same that the one followed for the model studied: some of the modes must be comparable to those obtained for the simulation model and the proportions must be similar to an actual aircraft. Also, an experimental procedure must be set to obtain the modes. This experimental procedure will be based on the actual methodology that is carried out in industry to certificate an aircraft, the ground vibration test (GVT). With the experimental modes and the modes obtained with FEM software an evaluation of the accuracy of the analysis can be conducted. In addition, the experimental model is intended to be used for teaching purposes at the University.

1.3 Gust Overview

One of the main objectives of the thesis is to evaluate the response of the aerodynamic loads in presence of a vertical gust. A gust is any component of the air velocity that varies the incidence of the aerodynamic surfaces and the magnitude of the dynamic pressure, giving rise to changes in aerodynamic forces and causing deformation of such surfaces due to structural flexibility.

The modelling of the gust is carried out with a simplified approach. Such approach includes the following assumptions: rigid aircraft, no aircraft response to the gust and steady aerodynamics. Then, the load factor produced on the aircraft in presence of a gust is:

$$n_z = \frac{1}{2}\rho V_T^2 \frac{C_{L_\alpha}}{W/S}(\alpha_0 + \Delta\alpha) \tag{1.1}$$

where the terms that vary according to the shape of the gust are:

$$\begin{aligned} V_T^2 &= (V_0 + W_g cos\theta))^2 + W_g^2 sin^2\theta \\ \Delta\alpha &= arctan\left(\frac{W_g sin\theta}{V_0 + W_g cos\theta}\right) \end{aligned} \tag{1.2}$$

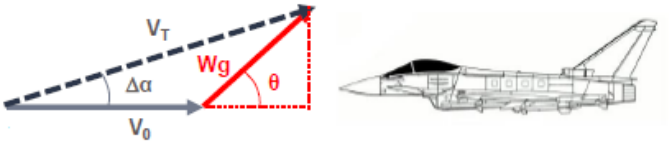

Figure 1.1: Gust contribution [9]

The load factor varies with these terms according to figure 1.2:

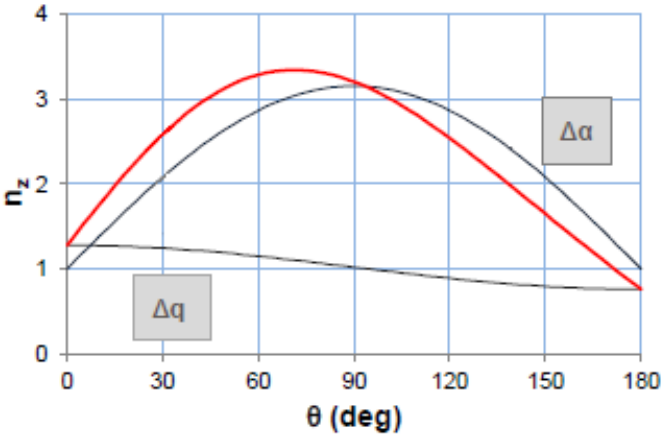

Figure 1.2: Gust variation [9]

Figure 1.2 shows that the variation of the dynamic pressure has limited effect on the magnitude of the load factor compared to the impact of the variation of the angle of attack. Nevertheless, the effect of the dynamic pressure is still significant when determining the critical gust profile since the curve is shifted to the left, changing the gust direction. In this condition, the critical gust takes place when it has an angle of 70-80° instead of 90° (condition at which the contribution of $\Delta\alpha$ is maximum). Meanwhile, for simplicity, in the analysis the contribution of the dynamic pressure is going to be neglected, implying that the gust studied will be a vertical gust with no velocity component in the x-direction.

The reason to account for the effect that a gust may have in the loads experienced by the aircraft is that gust conditions involve limiting loads in some structural components of the aircraft. Gust inclusion must be studied in order to design the aircraft to withstand the maximum loads that might appear during aircraft lifetime. The components of the aircraft in which critical gust is the dimensioning case are:

- Wing shear force (F_z) & bending moment (M_x)

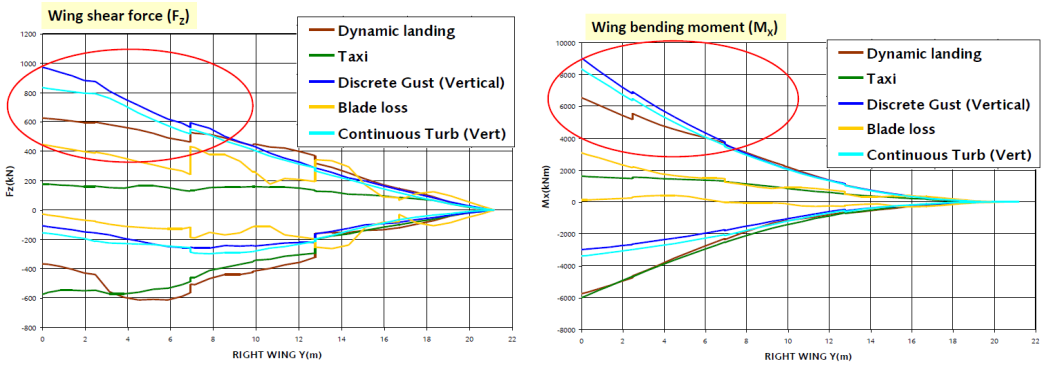

(a) Wing shear force (b) Wing bending moment

Figure 1.3: Wing sizing [9]

- Fuselage shear force (F_z) & VTP shear force (F_y)

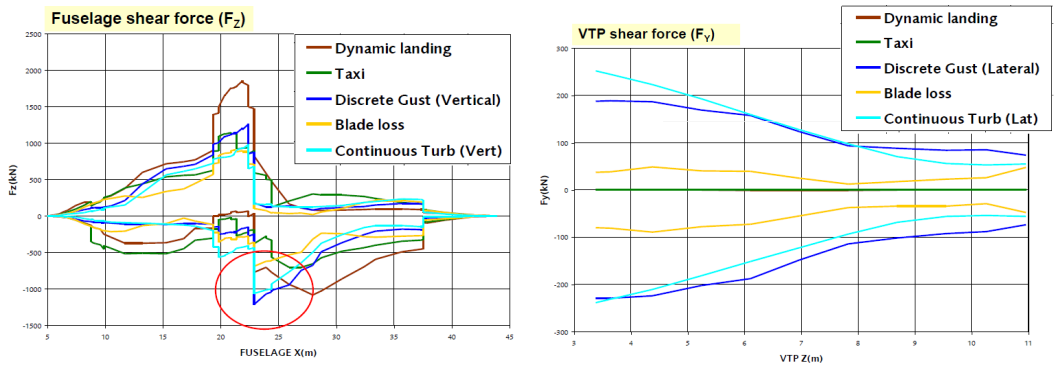

(a) Fuselage Sizing (b) VTP Sizing

Figure 1.4: Aircraft sizing [9]

Figures 1.3 and 1.4 prove that the analysis of the critical gust contribution to the loads experienced by the aircraft is fundamental for the correct and safe sizing of the concerning aircraft parts.

Gusts have three different contributions on the aircraft that make it differ from the ideal assumption (change in the effective angle of attack):

1. **Structural flexibility effect**

Due to structural flexibility, when external loads are applied to the lifting surfaces, elastic twist and surface bending are induced, changing the shape of the surfaces and their aerodynamic performance [35]. The effect of the structural flexibility can have two different impacts:

- Increase of the aerodynamic loads: this effect takes place when the twist induced is positive (nose-up). This twist increases the angle of incidence, being this one larger when compared to the angle of incidence of rigid surfaces. This effect is generally produced when the shear center is located backward (further to the leading edge) from the center of pressure.

- Decrease of the aerodynamic loads: this effect is the opposite to the previous one, a negative twist (nose-down) is produced, decreasing the angle of incidence. This twist is usually generated when the shear center is located forward (closer to the leading edge) from the center of pressure.

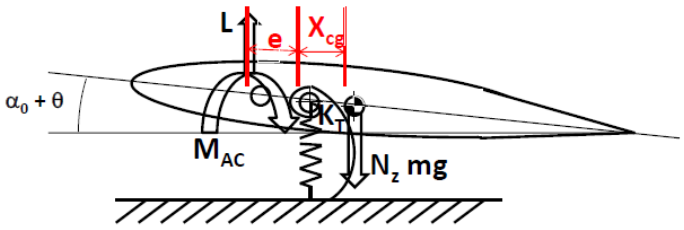

Figure 1.5: Elastic twist due to C_p location [7]

In figure 1.5, e is the distance from the center of pressure to the elastic axis (shear center) of the airfoil, X_{cg} is the distance from the center of gravity to the elastic axis, M_{ac} is the moment at the aerodynamic center, L is the lift, N_z is the load factor, m is the mass, g is the acceleration of gravity, K_T is the torsional stiffness, θ is the elastic twist produced by the aerodynamic loads and α_0 is the geometric angle of attack of the airfoil. Furthermore, the elastic twist of the wing also depends on the position of the center mass of the wing in

relation to the elastic axis, since the weight of the wing affects likewise to the torsion and bending. The elastic twist generated by the aerodynamic loads and the weight of the wing can be expressed in terms of the following equation:

$$M_{ac} + L \cdot e + N_z mg \cdot X_{CG} = K_T \theta \tag{1.3}$$

2. **Rigid-body motion of the aircraft**

When including an uniform gust, the lift produced by the lifting surfaces increases, this generates an upwards acceleration of the aircraft. This increase in vertical velocity (V_v) decreases the effective angle of attack of the surfaces. Therefore, it can be stated that the rigid-body motion always reduces the net effect of the gust.

$$\Delta\alpha = arctan\left(\frac{W_g - V_v}{V_c}\right) \tag{1.4}$$

3. **Unsteady Aerodynamics**

Unsteady aerodynamics effect includes the fact that the change in lift produced by a gust does not occur instantaneusly, the variation in lift increases gradually until it reaches the steady value.

Aircraft response to the change in angle of attack due to a step gust, i.e. the one studied in this work, is represented by Wagner's function. Wagner's function expresses the lift produced due to a sudden change in the angle of attack. This lift would vary half its value instantaneusly and it would increase from this point to the final value of the lift asymptotically. Wagner's equation expresses the lift as:

$$L = L_{steady}\phi(s) \tag{1.5}$$

where $\phi(s)$ is Wagner's function which depends on the distance travelled in semi-chords.

Normalizing the lift such that the initial value is equal to unity, the response to a sudden change of the angle of attack ($\Delta\alpha = \alpha_0/2$) as a function of the distance covered is represented in figure 1.6 for both unsteady and quasi-steady cases:

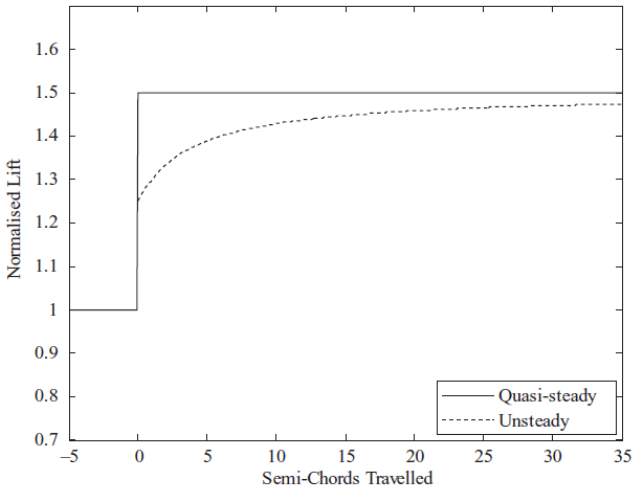

Figure 1.6: Wagner's function [7]

Figure 1.6 shows that the lift variation reaches half its value instantaneusly, while the final value is reached asymptotically.

In this thesis, the effect that is going to be studied is the first one, i.e. the impact of structural flexibility. On the other hand, the vertical motion of the aircraft is not going to be included in the analysis and, as well, the evaluation is going to be performed in quasi-steady conditions so that the change in aerodynamic forces is considered instantaneous.

In the case that structural flexibility has a beneficial effect on the loads generated by the presence of a gust, studying this effect may imply a reduction of the strength requirements of the structure since structural flexibility may provoke lower loads than considering rigid structures. This effect would allow to make thinner structures or reduce the number of structural joints, decreasing the weight and operational cost of the aircraft. On the other hand, if structural flexibility has a detrimental effect on the loads produced by a gust when compared with rigid structures, the loads generated would be larger than expected, so the analysis of this effect would be fundamental to know exactly the limits of the structure in these conditions.

1.4 GVT

The GVT is a non-destructive structural test carried out on-ground on an aircraft ready to fly with the objective of obtaining the normal modes of the aircraft. The experimental modes obtained in the GVT allow to update the dynamic FEM model until the results match and, thus, the model can be considered valid. This test is primordial to clear the aircraft for flight, planning carefully this test is essential for any aircraft manufacturing and validating processes [8].

The prototype that is tested must be "ready to fly", this condition implies:

- Electric and hydraulic systems installed.
- Aircraft primary structure completed.
- Engines installed.
- Operative control surfaces.
- Fuel tanks installed and sealed.

Not only the aircraft must be ready for flight, but also the aircraft must be tested in all those configurations that present significant differences.

A fundamental part of the GVT is that the test should give modes comparable to those that take place in real aircraft operation. With a view to achieve similar results, the boundary conditions at which the aircraft is tested must be as close as possible to free-free conditions. There are different solutions to model these conditions:

- Aircraft on bungees: method that provides the most precise solution to model free-free boundary conditions.
- Pneumatic platforms: still quite precise but they add some uncertainty to the damping of the rigid body modes.
- Deflacted tires: it is useful for modified models but it is not recommended for new designs.
- Aircraft on jacks: not recommended due to the uncertainty on the stiffness induced by the jack.

Once the aircraft and the boundary conditions have been defined, the measurement devices must be set prior to model excitation. The measurements of the modal frequencies are obtained by means of accelerometers located over the prototype structure. These accelerometers are connected by cables to the acquisition system that reads the signal. Then, the signal is processed to suppress the noise that may appear and to remove any possible error in the measurements.

Lastly, to obtain the signal the prototype must be excited. The methods used to excite the aircraft are several:

- Electrodynamic exciters (shakers).
- Using control surfaces (Flight Vibration Test).
- Operating the aircraft (Operational Modal Analysis).
- By hand (useful for low-frequency rigid body modes).

- Instrumented impact hammer.
- Hydraulic exciters.

The best option, and preferred, is to use shakers applying energy in all axes without damaging the structure and avoiding noise. Subsequently, the excitation is performed by sweeping frequencies within a specific range where the aimed mode frequency is expected to be located.

1.5 Project Timeline

The project must have a clear and strict timetable that presents the major procedures performed in this thesis in order to organize the required time expected for each task and to be able to finish in the aimed deadline. The following diagram includes all the major aspects of the analysis and the time during which they are be performed:

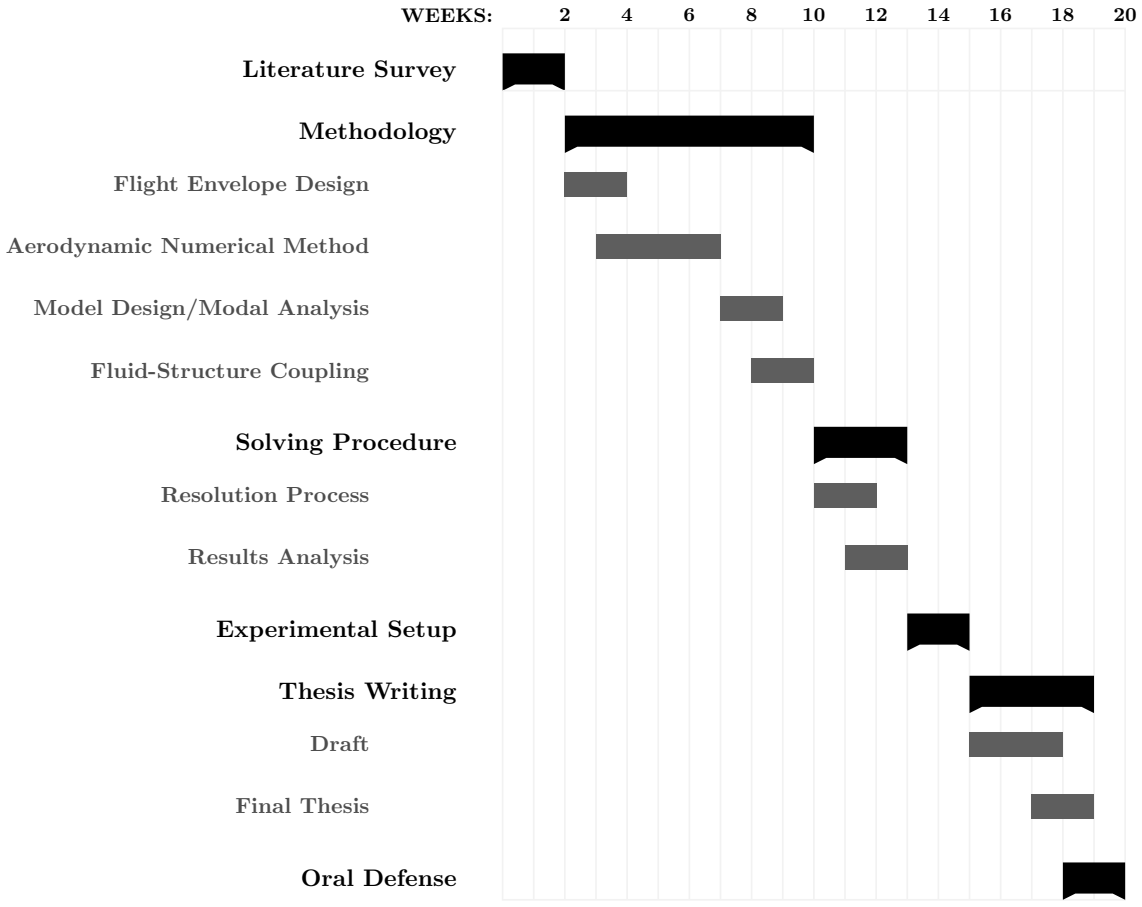

1.6 Thesis Structure

In chapter 2, the regulations that apply to the problem studied are analysed. In chapter 3, the conditions and methods used to perform the assessment of the effect of structural flexibility on loads are explained. In chapter 4, the different designs evaluated are described together with the assumptions made concerning the FEM model. In chapter 5, the results of the main parameters related to structural flexibility of the aircraft are exposed and the analysis of these results is performed. In chapter 6, the experimental setup required to perform a GVT of the specimen designed is proposed. In chapter 7, an evaluation of the potential socio-economic impact of structural flexibility and the budgets of this investigation and the experimental modal analysis test are presented. In chapter 8, the main conclusions obtained are summarized.

Chapter 2

Regulatory Framework

Before implementing the aerodynamic and structural models, the flight conditions at which the analysis is performed must be determined. The first condition that should be specified is the cruise altitude. For simplicity, as some of the following conditions will be obtained in terms of EAS, the analysis will be assumed to take place at sea level conditions. The other flight characteristics required to carry out the analysis are the cruise speed and the critical gust. Nevertheless, these conditions cannot be determined directly since both of them have restrictions corresponding to those established by EASA (in the case of aircraft flying in Europe) and these must be fulfilled in order to validate aircraft operation.

The prototype designed and studied has dimensions similar to an UAV so it would be logic to define the flight characteristics in accordance with the corresponding official regulations. Nevertheless, these regulations do not include any reference to cruise and gust conditions. In order to obtain specific results and not to simply invent these values, a different regulation will be used as an approximation and the values obtained will be applied to our model.

From the actual certification regulations of EASA, the one that best matches to an UAV characteristics is the CS-VLA [11] which groups aeroplanes with a MTOW lower than 750 kg. However, as it is not specific for UAVs with the size of the model studied, a second approach will be followed to compute the $\Delta\alpha$ induced by the gust. This second approach is based in obtaining the $\Delta\alpha$ for a bigger airplane (C-295) but applying the right regulations (CS-25 [10]). Following this procedure, the analysis covers two different methods to account for the scatter induced by using regulations that do not cover the actual model.

Although the previous methods are going to be carried out, the cruise speed is only going to be determined by using CS-VLA instead of considering both since CS-25 would give a velocity too high for an UAV of this size. Nevertheless, both methods will be applied for the computation of the critical gust.

2.1 Cruise Speed

The cruise speed must be fixed in order to perform the aerodynamic iteration process that will be explained later on. Such speed has a lower and upper limit regarding the CS-VLA regulations. The definition of these limits can be found in CS-VLA paragraph 335: Design Airspeeds.

- Minimum V_c (cruise speed):

$$V_{c,min} \geq 4.7\sqrt{\frac{W}{S}} \tag{2.1}$$

where $V_{c,min}$ is in knots and W/S is the wing loading in N/m^2. The weight used will be the obtained from the model designed. The weight of the model is 133 N. On the other hand, the surface of the wing is 0.5 m^2. All this data gives as minimum cruise velocity: $V_{c,min} = 76.65\ kts\ = 39.43\ m/s$.

- Maximum V_c

$$V_{c,max} \leq 0.9V_H \tag{2.2}$$

where V_H is the maximum velocity in level flight with maximum continuous power. However, the propulsion of the model is not one of the aims of this study so the maximum velocity cannot be computed. For this reason, the cruise velocity selected would be close to the minimum one, in this way an achievable cruise velocity can be assured and divergence phenomena (occurs when the aircraft reaches a specific velocity) can be avoided. The cruise velocity selected for the analysis is:

$$\mathbf{V_c = 40\ m/s}$$

2.2 Critical Gust (CS-VLA)

As explained previously, the static analysis of the aircraft is to be performed in both cruise flight and with the inclusion of a gust. The gust considered will be the one assumed to be the most critical that the aircraft may suffer. The shape of the critical gust will be defined by using the CS-VLA paragraph 333: Flight envelope-Part (c) Gust envelope. From this paragraph the following equation is obtained:

$$U = \frac{U_{de}}{2}\left[1 - cos\left(\frac{2\pi S}{25\overline{c}}\right)\right] \tag{2.3}$$

where U_{de} is the gust velocity given in subparagraph (c)(1) in m/s, S is the distance penetrated into gust in m., and $\bar{c}$ is the mean aerodynamic chord of the wing in m. As the model is analysed in quasi-static conditions, the critical gust is going to be assumed uniform with an amplitude equal to the maximum gust shape, therefore the gust shape will coincide with the given gust velocity, U_{de}.

According to subparagraph (c)(1), flying at cruise velocity (which is the case studied), the gust velocity that must be considered for the analysis is 15.24 m/s. Such gust will be included in the aerodynamic model as a contribution to the angle of attack, which can be expressed as a function of the terms obtained in previous sections:

$$\Delta\alpha = arctan\left(\frac{U_{gust}}{V_c}\right) = 20.857^{\circ} \tag{2.4}$$

2.3 Critical Gust (CS-25)

Meanwhile, the critical gust of the C-295 will be computed by using the CS-25 which are the regulations that must be applied to this aircraft. The $\Delta\alpha$ obtained will be implemented directly to our model to perform the analysis. Hence, the first step is to define the characteristics of a C-295 [13].

MTOW (kg)	21000
MLW (kg)	20700
MZFW (kg)	18500
OEW (kg)	13374
Maximum Operating Altitude (ft)	25000
Cruise Speed at SL (m/s)	126

Table 2.1: C-295 specifications

With the characteristics reported in table 2.1 it is possible to determine the critical $\Delta\alpha$ for the C-295. Nevertheless, prior to computing $\Delta\alpha$, some intermediate calculations must be performed as stated in CS 25.341: Gust and turbulence loads. The first task is to compute two weight ratios:

$$\begin{aligned} R_1 &= \frac{MLW}{MTOW} = 0.9857 \\ R_2 &= \frac{MZFW}{MTOW} = 0.8810 \end{aligned} \tag{2.5}$$

Secondly, the flight profile alleviation factor (F_g) must be obtained. This factor increases linearly from SL to a value of 1 at the maximum operating altitude (Z_{mo}). As the flight

conditions are at SL, the corresponding flight profile alleviation factor becomes:

$$F_{gz} = 1 - \frac{Z_{mo}}{250000} = 0.9$$

$$F_{gm} = \sqrt{R_2 tan\left(\frac{\pi R_1}{4}\right)} = 0.9281 \tag{2.6}$$

$$F_g = 0.5\left(F_{gz} + F_{gm}\right) = 0.9141$$

Note that the expression for F_{gz} is for Z_{mo} in feet.

Prior to compute the design gust velocity(U_{ds}), the reference gust velocity in EAS must be obtained. As the flight takes place at SL, the TAS and EAS are the same for this case. According to sub-paragraph (a)(5) of the CS 25.341, the reference velocity (U_{ref}) when flying at cruise speed (V_c) and at SL conditions is 17.07 m/s EAS. Then, the design gust velocity can be expressed as:

$$U_{ds} = U_{ref} F_g \left(\frac{H}{350}\right)^{1/6} \tag{2.7}$$

where H is the gust gradient, the distance (feet) parallel to the aircraft's flight path for the gust to attain its maximum velocity. The range of this term goes from 30 ft to 350 ft. Assuming that the critical gust coincides with the maximum design gust velocity, the gust gradient would be 350 ft and the design gust speed is:

$$U_{ds} = U_{ref} F_g = 15.60\ m/s \tag{2.8}$$

According to sub-paragraph (a)(2) of the CS 25.341, the shape of the gust is:

$$U_{gust} = \frac{U_{ds}}{2}\left[1 - cos\left(\frac{\pi s}{H}\right)\right] \tag{2.9}$$

where s is the distance penetrated into the gust in feet. However, as it was explained in the introduction, the analysis performed is quasi-static which implies that the critical gust corresponds to the maximum value of its velocity, obtaining:

$$U_{gust} = U_{ds} = 15.60\ m/s \tag{2.10}$$

Al last, the $\Delta\alpha$ produced by the critical gust becomes:

$$\Delta\alpha = arctan\left(\frac{U_{gust}}{V_c}\right) = 7.060^{\circ} \tag{2.11}$$

Chapter 3

Methodology

3.1 Axes Definition

For this analysis the first step that must be done is to define the axes and the directions of the forces that will appear along different sections of the study. The reference frame used will be body fixed reference frame so that its axes are placed as in figure 3.1:

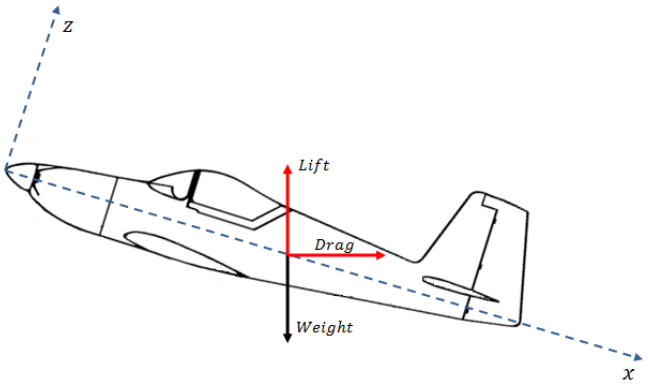

Figure 3.1: Axis and forces definition

Once the reference frame has been defined, and setting that the right hand rule is fulfilled, force and moment components can be determined according to this reference frame; also, the conditions that govern the aerodynamics and structural characteristics of the model can be implemented taking as reference the axis and directions defined in this section.

3.2 Flight Mechanics

Flight mechanics is the field of aerospace engineering that studies the motion of the aircraft assuming the aircraft is a rigid body. Within the motion of the aircraft different aspects are included as stability, performance and response. Aircraft flight mechanics also study the

natural modes of the aircraft as rigid body (phugoid, short period, rolling, spiral and dutch roll) together with different approaches for the control of this motion.

Nevertheless, the flight mechanics concepts applied in this study are not based on the aircraft response to those modes either to control mechanisms, the concepts used are based on simpler aspects concerning aircraft motion.

The first aspect that is introduced is the cruise condition. In cruise, the lift generated by the lifting surfaces must be equal to the weight of the aircraft in order to not vary the altitude. In real application the weight of the aircraft varies due to fuel consumption. However, in this study, fuel is not being included, for that reason the weight of the aircraft will be equal to the structural weight.

The condition of lift equal weight implies the following relation:

$$W = L = L_{wing} + L_{HTP} = \frac{1}{2}\rho U_{\infty}^2 \left(S_{wing} C_{L,wing} + S_{HTP} C_{L,HTP}\right) \tag{3.1}$$

Albeit the cruise condition is fulfilled with the previous expression, the lift generated by each surface is not fixed, another condition must be implemented to fix those values. The condition applied is based on the longitudinal stability of the aircraft. This condition states that, in order to have longitudinal equilibrium, the sum of moments around the center of gravity is zero so that the aircraft does not show pitch motion. The forces and moments exerted on the aircraft are illustrated in figure 3.2.

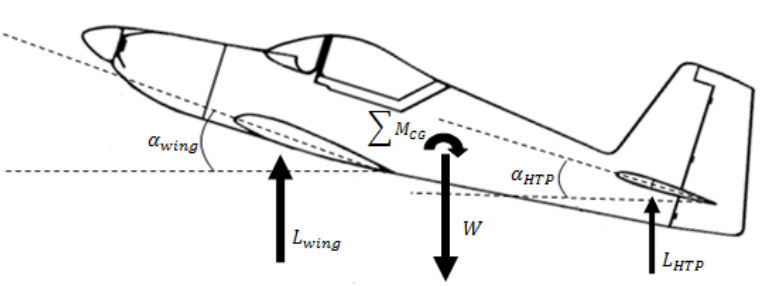

Figure 3.2: Aircraft longitudinal stability

The equation that models this condition is:

$$\sum M_{CG} = L_{wing}\left(x_{CG} - x_{CP,wing}\right) + L_{HTP}\left(x_{CG} - x_{CP,HTp}\right) = 0 \tag{3.2}$$

where x_{CG} refers to the center of gravity of the aircraft (obtained from ANSYS Design module) and x_{CP} refers to the center of pressure of the lifting surface: is the average location

of the pressure present on the surface so that exerting the resultant of the pressure field in that location is equivalent to exerting the pressure in its real place. The center of pressure of the wing can be computed with the following expression:

$$x_{CP} = \frac{\int x \cdot p(x)}{\int p(x)} \simeq \frac{\sum x \cdot p(x)}{\sum p(x)} \tag{3.3}$$

Although in subsonic flow the aerodynamic center is located at, approximately, 25% of the chord, the center of pressure may vary its position depending on the airfoil that forms the wing and HTP. For that reason the previous equation is included in the aerodynamic model in order to obtain the exact position of the center of pressure of each lifting surface.

Once these conditions have been defined the specific lift generated by the surfaces can be determined and the aerodynamic model can be implemented inasmuch as it fulfils the conditions. However, an important assumption must be taken into account prior developing the aerodynamic model: in actual aircrafts the longitudinal equilibrium condition is controlled by means of the deflection of the elevators located in the HTP; nevertheless, for simplicity, elevators are not considered in this studied so, in order to fulfil previous conditions, the HTP is going to be assumed that can rotate around y-axis and it can have a different angle of incidence than the wing, being able to generate lift as a function of the equations written in this section.

3.3 Aerodynamic Analysis

In order to perform the static analysis and determine the effect of structural flexibility on wing loading, the forces that are generated during flight must be studied. To do so, an aerodynamic model of both wing and HTP is designed in Matlab based on a 3D numerical panel method.

An adecuate number of panels must be chosen to reduce the error but it should suppose an acceptable computational cost to decrease the time needed for the study without decreasing the accuracy of the results.

3.3.1 Theoretical Background

The motion of a fluid is represented by the Navier-Stokes equations, a set of partial derivatives equations which do not have analytical solution except for certain and specific conditions.

Nonetheless, the flow around wing and HTP is going to be assumed potential flow. To achieve the potential equations of a fluid, the following assumptions must be applied to the Navier-Stokes equations:

- Adiabatic flow: there is no heat exchange.
- Viscosity effects negligible: $Re = \dfrac{\rho V D}{\mu} \gg 1$
- Gravity effects negligible: $Fr = \dfrac{v}{\sqrt{g D_h}} \ll 1$

These conditions give the Euler equations which still do not represent a potential flow.

A flow is defined as potential when it is irrotational, that means that the vorticity ($\overline{\omega} = \nabla \wedge \overline{V}$) is zero at every point of the flow. As well, in terms of simplicity, the flow is going to be modelled as incompressible and quasy-steady, giving as resultant equations [2]:

$$\overline{V} = \nabla \phi \tag{3.4}$$

$$\nabla^2 \phi = 0 \tag{3.5}$$

where ϕ is the velocity potential, ∇ is the gradient and ∇^2 is the Laplacian operator. The boundary conditions are applied far away from the body and on the wall of it, respectively:

$$\begin{gathered} \lim_{|\overline{x}| \to \infty} \nabla \phi = U_\infty \overline{e}_x \\ \overline{V} \cdot \overline{n} = 0 \quad \text{on surface} \quad F(\overline{x}) = 0 \end{gathered} \tag{3.6}$$

where $\overline{n}$ corresponds to the vector normal to the surface, in such a manner that it can be expressed as $\dfrac{\nabla F}{|\nabla F|}$ and U_∞ is the free stream velocity.

Once the equations and the boundary conditions have been defined, the boundary condition at the body can be determined. First, the velocity potential is expressed to satisfy equation (3.5):

$$\phi = U_\infty cos(\alpha) x + U_\infty sin(\alpha) z + \varphi \tag{3.7}$$

where φ is the perturbation potential, which represents the effect of the surface on the flow. On the other hand, α represents the angle of attack of the surface. With the velocity potential, the velocity can be obtained:

$$\overline{V} = \nabla \phi = \left(U_\infty cos(\alpha) + \frac{\partial \varphi}{\partial x} \right) \overline{e}_x + \left(\frac{\partial \varphi}{\partial y} \right) \overline{e}_y + \left(U_\infty sin(\alpha) + \frac{\partial \varphi}{\partial z} \right) \overline{e}_z \tag{3.8}$$

Now, the remaining term necessary to determine the boundary condition at the body is the vector normal to the surface. Thus, first the surface must be defined:

$$F(\overline{x}) = z - \eta(x, y) A - h(x, y) \tag{3.9}$$

where $h(x, y)$ is the vertical position due to elastic deformation, $\eta(x, y)$ is the camber plus the thickness at a specific point of the body (perpendicular to the body) and A is a coefficient

that corrects the difference between the camber plus the thickness of the surface with the actual vertical distance at that point (it is graphically represented in figure 3.3):

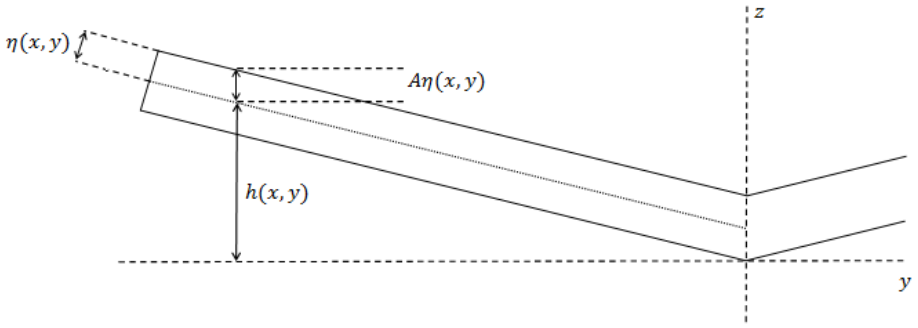

Figure 3.3: Vertical distance correction

where A corresponds to the z-component of the vector normal to the surface of the panel (as shown in figure 3.3).

Then, once the surface has been defined, the vector normal to such surface can be obtained:

$$\overline{n} = \frac{\nabla F}{|\nabla F|}$$

$$\frac{\nabla F}{|\nabla F|} = \frac{\left[\left(-\frac{\partial h}{\partial x} - A\frac{\partial \eta}{\partial x}\right)\overline{e}_x,\ \left(-\frac{\partial h}{\partial y} - A\frac{\partial \eta}{\partial y}\right)\overline{e}_y,\ 1\overline{e}_z\right]}{\left(\sqrt{\left(-\frac{\partial h}{\partial x} - A\frac{\partial \eta}{\partial x}\right)^2 + \left(-\frac{\partial h}{\partial y} - A\frac{\partial \eta}{\partial y}\right)^2 + 1}\right)} \tag{3.10}$$

The boundary condition at the wall of the bodies is expressed in terms of $h(x, y)$; the camber of the airfoil (thickness is neglected because it does not affect the lift problem), η; the angle of attack, α; the free stream velocity, U_∞; and the perturbation potential, φ:

$$\begin{aligned}\overline{V} \cdot \overline{n} = \Bigg[&\left(U_\infty cos(\alpha) + \frac{\partial \varphi}{\partial x}\right)\left(-\frac{\partial h}{\partial x} - A\frac{\partial \eta}{\partial x}\right) + \\ &+ \left(\frac{\partial \varphi}{\partial y}\right)\left(-\frac{\partial h}{\partial y} - A\frac{\partial \eta}{\partial y}\right) + \left(U_\infty sin(\alpha) + \frac{\partial \varphi}{\partial z}\right)\Bigg]\frac{1}{|\nabla F|} = 0\end{aligned} \tag{3.11}$$

From this equation the following assumptions are applied:

$$\begin{gathered}U_\infty \gg \frac{\partial \varphi}{\partial x},\ \frac{\partial \varphi}{\partial y},\ \frac{\partial \varphi}{\partial z} \longrightarrow \frac{\partial \varphi/\partial x}{U_\infty},\ \frac{\partial \varphi/\partial x}{U_\infty},\ \frac{\partial \varphi/\partial x}{U_\infty} \sim \epsilon \ll 1 \\ A\frac{\partial \eta}{\partial x},\ A\frac{\partial \eta}{\partial y} \sim \epsilon \ll 1\end{gathered} \tag{3.12}$$

Under these assumptions, the boundary equation at the wall can be defined as:

$$(U_\infty cos(\alpha) + \epsilon U_\infty)\left(-\frac{\partial h}{\partial x} - \epsilon\right) + (\epsilon U_\infty)\left(-\frac{\partial h}{\partial y} - \epsilon\right) + (U_\infty sin(\alpha) + \epsilon U_\infty) = 0 \quad (3.13)$$

Keeping only those terms of order ϵ or greater and defining $\frac{\partial \varphi}{\partial x} = u'$, $\frac{\partial \varphi}{\partial y} = v'$, $\frac{\partial \varphi}{\partial z} = w'$, the resulting expression that will be used for the boundary condition at the wall is:

$$U_\infty\left(-sin(\alpha) + \frac{\partial h}{\partial x}cos(\alpha) + A\frac{\partial \eta}{\partial x}cos(\alpha)\right) = w' - v'\frac{\partial h}{\partial y} - u'\frac{\partial h}{\partial x} \quad (3.14)$$

where $\frac{\partial h}{\partial x}$ represents the twist produced along the surface and $\frac{\partial h}{\partial y}$ the bending. Once the equations required to solve the aerodynamic model have been set, the numerical lifting surface method will be implemented to obtain the distribution of pressure and forces over the surfaces.

3.3.2 Numerical Lifting Surface Method

The numerical lifting surface method consists of a finite and thin surface (wing and HTP) flying in an incompressible and undisturbed fluid. For the analysis, the flight conditions must be defined:

- Free stream velocity$\equiv U_\infty = 40$ m/s
- Sea Level Conditions $\longrightarrow \rho = 1.225$ kg/m^3

Also, the dimensions of the surfaces (contained in table 3.1) are required for the calculations:

Characteristic Measures	Wing	HTP
Span, b	2000 mm	600 mm
Chord, c	250 mm	200 mm
Aspect Ratio, AR	8	3

Table 3.1: Surface dimensions

With the necessary conditions and dimensions already set, the method can be implemented. The method is based on Katz, J. and Plotkin, A. [22] lifting surface solution by vortex ring elements.

The first step of the method consists of discretisizing the surface into panels. Although the flexibility of the surface produces curvature, the panels are defined as straight rectangular panels but small enough to reduce the curvature error. The number of panels used will be obtained later by comparing different panels distribution with the results obtained with XFLR5 software [36].

The panels are defined initially by a rectangular surface located in the $z = 0$ plane and adding later the displacements resultant from the deformation of the surface. Then, the collocation points (point where the induced velocity at each panel is computed) are located at the center of each panel.

The next step is to define the vectors perpendicular to each panel, which are needed for the computation of the aerodynamic coefficient matrix. These normal vectors are obtained with the cross product of the vectors that the define the surface of the panel (figure 3.4):

$$\overline{n}_k = \frac{\overline{d}_{x,k} \times \overline{d}_{y,k}}{|\overline{d}_{x,k} \times \overline{d}_{y,k}|} \tag{3.15}$$

where k designates a specific panel.

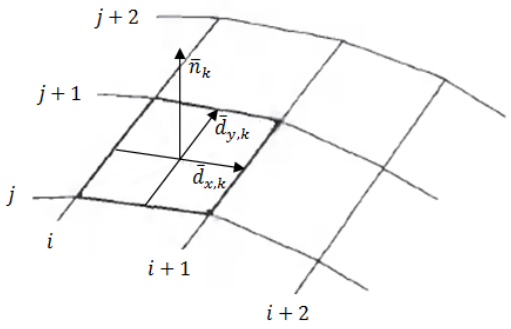

Figure 3.4: Vector normal to panel

Lastly, prior to placing the singularities on the panels, the normal velocity at each panel must be computed for later calculation of the circulation. As it was shown in the theoretical background, the velocity has three main components besides the free stream velocity: the angle of attack, α, which is defined by the flight mechanics conditions; A $\left.\frac{\partial \eta}{\partial x}\right|_k$ and $\left.\frac{\partial h}{\partial x}\right|_k$ which are defined at each panel. This last term can be easily obtained with straight rectangular panel approximation:

$$\frac{\partial h}{\partial x} = \frac{\Delta h}{\Delta x} = \frac{z_{i,j+1} - z_{i,j}}{x_{i,j+1} - x_{i,j}} \tag{3.16}$$

where the sub-index i denotes panel position in x-direction and the sub-index j denotes panel position in y-direction. Furthermore, the camber of the airfoil along the chord, $\eta(x)$, is defined by the following expressions[1]:

$$\begin{aligned} &For\ 0 \leq \overline{x}_{i,j} < P && \eta_{i,j}(x) = \frac{M}{P^2}\left(2P\overline{x}_{i,j} - \overline{x}_{i,j}^2\right) \\ &For\ P \leq \overline{x}_{i,j} < 1 && \eta_{i,j}(x) = \frac{M}{1-P^2}\left(1 - 2P + 2P\overline{x}_{i,j} - \overline{x}_{i,j}^2\right) \end{aligned} \tag{3.17}$$

[1]Equations obtained from: `http://airfoiltools.com/airfoil/naca4digit`. Accessed: 12/03/2016

where c is the chord length, $\overline{x} = x/c$, P is the maximum camber position divided by 10 and M is the maximum camber divided by 100.

Then, the induced velocity perpendicular to each panel is expressed as the left hand side of equation (3.14).

After following the previous steps, the placing of the singularities can be carried out. From Green's identity formula it is obtained that the surface must be modelled with vortices and sources, while the wake can be modelled only with vortices. Nevertheless, the sources placed on the wing represent the thickness effect, which is negligible in the lift problem. As the results that this model aims are the vertical forces and the difference of pressure between the top and bottom of the surface, the wing and HTP can be modelled only with vortices.

Two main solutions can be applied to represent the vortices: the vortex ring and the horseshoe element. The vortex ring method would locate vortices on the sides of the panels while the horseshoe vortex would locate vortices on the head edge of the panel and infinite vortex lines coincident with the sides of the panel as shown in figure 3.5. Then, the influence of every panel of the surface on each collocation point is computed until all points have been covered. Both methods are valid, nevertheless, in a surface which presents twist and bending, i.e. the ones studied, the horseshoe vortex becomes inadequate as its legs must be parallel to the flow (due to the twist this does not happen). However, the surface cannot be modelled only with vortex rings as then the wake would not be represented.

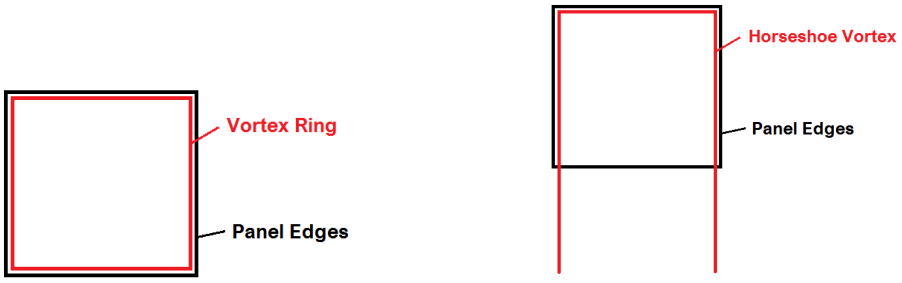

(a) Vortex Ring Element (b) Horseshoe Vortex Element

Figure 3.5: Vortex elements setting

The solution assumed as most efficient is to combine both methods. All the panels of the surface will be modelled as vortex rings whose sides coincide with the edges of each panel, except for those ones that are located in the trailing edge which will be modelled as 5-legs-horseshoe vortex elements whose sides are defined as: one coinciding with the front edge of the panel, other two coinciding with the lateral edges and the last two are defined such that are parallel to the flow (modelling the wake effect). Figure 3.6 illustrates the method applied.

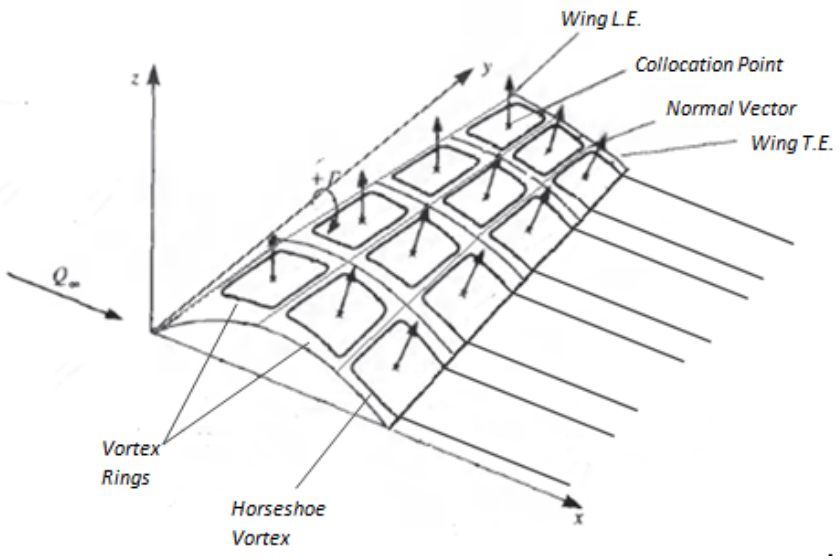

Figure 3.6: Numerical panel method [22]

The vortex ring and the horseshoe element are implemented applying a unit strength vortex in such a manner that the result corresponds to the aerodynamic influence coefficient matrix. In the influence coefficient matrix, $c_{k,m}$ represents each element of the influence coefficient matrix, $[C]$; sub-index k denotes the collocation point and sub-index m refers to the panel whose vortices induce a velocity $(r, s, t)_{i,j}$ on the collocation point k. Therefore the size of the matrix will be $K \times K$, being K the total number of panels. Nevertheless, from this method three terms, each one corresponding with an induced velocity component, are obtained. In order to get the coefficient, this vector must be projected into the normal of the panel so that:

$$c_{k,m} = (r, s, t)_{i,j} \cdot \overline{n}_k \tag{3.18}$$

To compute the forces and pressure over the surfaces, the circulation at each panel, Γ_k, must be obtained. To do so the following expression is applied:

$$[C]\{\Gamma_k\} = U_\infty \left(-sin(\alpha) + \left.\frac{\partial h}{\partial x}\right|_k cos(\alpha) + \left.\frac{\partial \eta}{\partial x}\right|_k cos(\alpha) \right) \tag{3.19}$$

Once the circulation of each panel has been computed the normal force at each panel is obtained applying the Kutta-Joukowski theorem:

- Panels at the leading edge

$$N_{1,j} = \rho \Gamma_{1,j} U_\infty \Delta y_{1,j} \tag{3.20}$$

- Remaining panels

$$N_{i,j} = \rho \left(\Gamma_{i,j} - \Gamma_{i-1,j} \right) U_\infty \Delta y_{i,j} \tag{3.21}$$

where, in this case, the sub-index i denotes the location of the panel in x-direction and sub-index j denotes the location of the panel in y-direction. In previous equations Δy represents the spanwise length of each panel. Hence, the pressure difference, which is the data that is going to be exported to ANSYS, becomes:

$$\Delta P_k = \frac{N_k}{\Delta x_k \Delta y_k} \tag{3.22}$$

where Δx is the chordwise length of each panel.

3.3.3 Panels Sensitivity Analysis

Now that the method has been described and implemented in Matlab, the number and distribution of panels over both wing and HTP must be determined. The aim is to use the minimum number of panels that give a quite accurate result but, at the same time, reduces the computational cost. To check that the code is correct and which is the minimum number of panels, a surface with a specific dihedral and twist distribution is analysed and compared using as reference value the one obtained by using XFLR5 software. XFLR5 is used because it is useful to determine the accuracy of the method implemented by means of a validated aerodynamic solver. The surfaces (same dimensions than wing and HTP) have the following properties:

- A linear twist distribution from 0° at the root to 4° at the tip.
- A dihedral angle of $\phi_1 = 2°$ from the root to a quarter of the span, and $\phi_2 = 4°$ dihedral angle from quarter of the span to the tip (shown in figure 3.7).

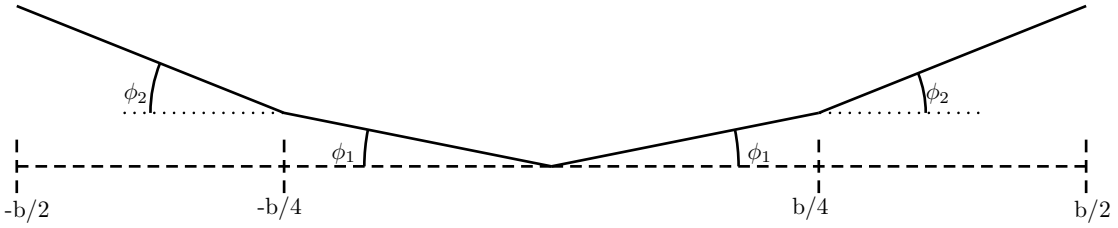

Figure 3.7: Surface design

The airfoil used is a symmetric airfoil (NACA 0012) so the results agree with those computed by the numerical lifting surface method.

The method applied in XFLR5 is the vortex ring method in inviscid flow at the same flight conditions that the ones stated before. The number of panels used in XFLR5 is such that doubling the number of panels it gives an equal result. The distribution of panels implemented is 220 panels in y-direction and 24 panels in x-direction and the resultant lift coefficient is used as reference value for the sensitivity analysis.

The procedure will consist of comparing the lift coefficient at different number and distribution of panels in the numerical lifting surface method with the lift coefficient obtained with XFLR5 software. Also, the time required for the solving process will be measured to compare computational cost with accuracy of the results. The comparison will be carried out for both wing and HTP. The results for the wing are gathered in table 3.2:

Panels-x	Panels-y	Total Panels	$C_L(\alpha = 0)$	Time (seconds)	Error (%)
10	80	800	0.1454	45	0.69
10	100	1000	0.1450	70	0.42
10	120	1200	0.1447	101	0.21
10	160	1600	0.1444	180	-
16	80	1280	0.1454	115	0.69
16	100	1600	0.1450	179	0.42
16	120	1920	0.1446	257	0.14
16	160	2048	0.1444	461	-
20	80	1600	0.1454	178	0.69
20	100	2000	0.1450	311	0.41
20	120	2400	0.1447	404	0.21
20	160	3200	0.1444	719	-
	XFLR5		0.1444	-	-

Table 3.2: Wing aerodynamic mesh

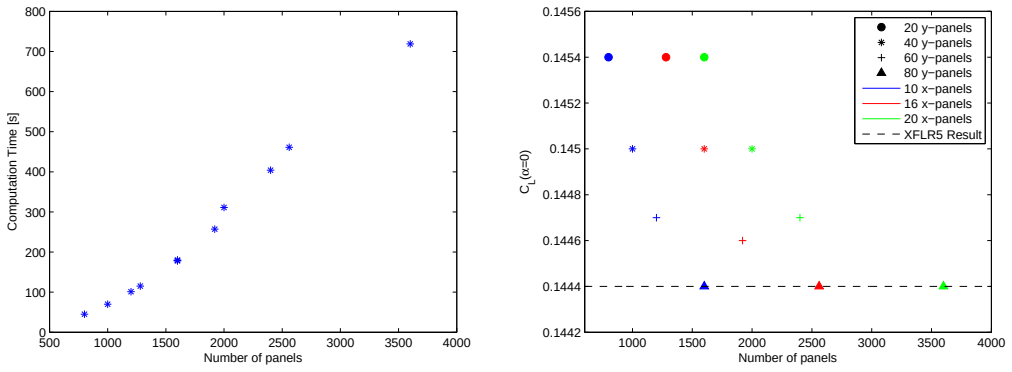

(a) Time study (b) Accuracy study

Figure 3.8: Wing panels distribution analysis

Any result that has an error smaller than a 1% of the real value is acceptable since such error is assumable due to the increase on the computational cost required to reduce the inaccuracy. Nevertheless, as the aim of this code is not only to obtain a certain result but also to import the resultant data to other program, its inexactitude does also affect other calculations which will have as well some inherent error; due to this fact, the aim of the panels sensitivity analysis is to have a variation smaller than 0.5% so that it has a smaller impact in FEM software calculations.

Table 3.2 and figure 3.8(a) show that the computational time needed to solve the aerodynamics of the wing follows an exponential trend, so that the smallest possible number of panels is required such that the time required is reduced as much as possible. Also, another important fact shown by figure 3.8(b) is that increasing the number of panels in x-direction does not significantly alter the results, consequently 10 panels in x-direction would be the optimum option since increasing this number would not provide more accurate results but would increase the computational time. However, the number of panels in y-direction does vary the resultant lift coefficient, having this number to be 100 or larger to fulfil the condition of inducing an error smaller than a 0.5%. Then, the optimum distribution would be 100 panels spanwise and 10 panels chordwise. The same analysis is performed for the HTP:

Panels-x	Panels-y	Total Panels	$C_L(\alpha = 0)$	Time (seconds)	Error (%)
10	20	200	0.1005	3	5.07
10	40	400	0.0976	12	2.04
10	60	600	0.0967	26	1.10
10	80	800	0.0961	45	0.47
16	20	320	0.1005	7	5.07
16	40	640	0.0976	28	2.04
16	60	960	0.0966	64	0.99
16	80	1280	0.0961	114	0.47
20	20	400	0.1005	11	5.07
20	40	800	0.0976	44	2.04
20	60	1200	0.0966	97	0.99
20	80	1600	0.0961	179	0.47
XFLR5			0.0956	-	-

Table 3.3: HTP aerodynamic mesh

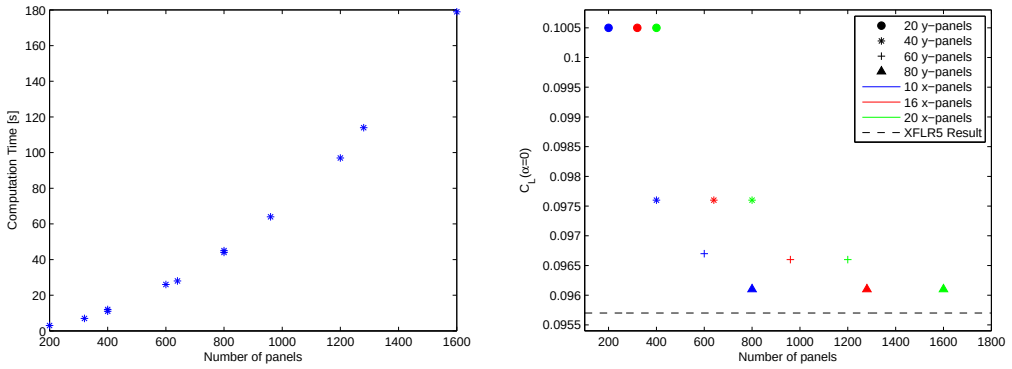

(a) Time study

(b) Accuracy study

Figure 3.9: HTP panels distribution analysis

As it happened with the wing, the computational time (table 3.3 and figure 3.9(a)) shows an exponetial curve as the number of panels increases. As well, increasing the number of panels in x-direction does not affect the results (figure 3.9(b)), so 10 panels chordwise would be again the best option to obtain an accurate result within a short time period. However, in this case, there are not many possiblities regarding the number of panels spanwise since the error of the results is lower than a 0.5% only using 80 panels in y-direction, giving as best distribution more than 80 panels spanwise and 10 panels chordwise.

Albeit the best panels distribution have been already determined, these must agree with the mesh implemented in ANSYS FEM (the same number of panels and distribution is used for the aerodynamic model and for the mesh of the structural analysis), so a similar mesh sensitivity analysis must be performed in ANSYS FEM prior definitely determining the panels distribution to be used.

3.4 ANSYS Finite Element Method

The software that is going to be used to solve both the modal and the static analyses is ANSYS FEM. ANSYS is a CAE (computer aided engineering) program which allows to solve problems that involve any physical aspect as: static structural, dynamic structural, modal, fluids, electrical, electromagnetic, electronic and thermal. In this project we will work with the structural module.

FEM is a mathematical tool to solve field problems, i.e., problems defined by an ODE that need to fulfil a set of boundary conditions. FEM was designed to solve problems that do not have analytical solutions or imply a complex solving process in which mistakes are easily made. FEM simplifies the problem by discretizising the model into elements which can be of

different size and shape. As higher is the number of elements, more accurate are the results as figure 3.10 shows.

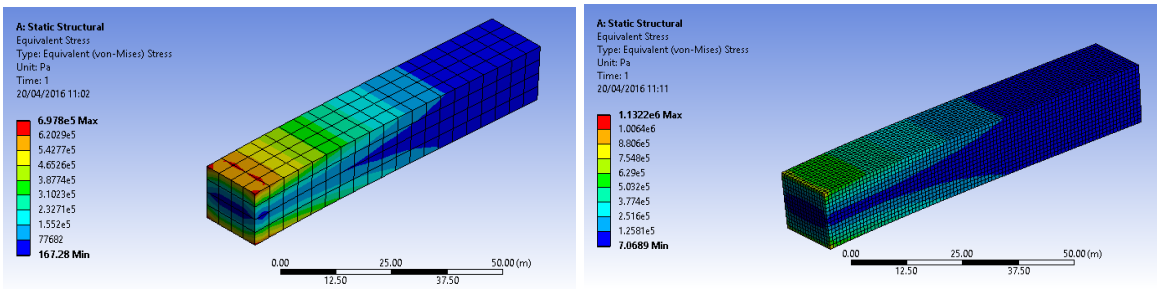

(a) Coarse mesh (b) Fine mesh

Figure 3.10: 3D model of a cantilever beam subjected to uniform pressure

These elements are connected between each other at points called 'nodes'. The manner in which FEM sofware solves the structural problem is by reducing the differential equations into a set of algebraric linear equations to obtain the displacement and rotation of the nodes; hence, the structure is reduced to a specific quantity of elements and presents a finite number of DoF.

In the case of aircraft structural modelling two main options can be applied for most of its components (fuselage, wingbox...): assuming these components as beams or defining the complete structural model (beam elements, membrane, bar, shell...). Although the model studied is going to be represented by solid elements, the purpose of this section is to make a brief introduction about FEM software so, for simplicity, a beam-like element is going to be the base of the explanation. This example is based on the methodology explained in [35]. The beam element is assumed as a 1D element with two degrees of freedom per node.

3.4.1 FEM solving of a beam element

Lets assume only the bending of a beam element which has the following properties: density ρ, flexural rigidity EI and length L. For simplicity, lets assume that it is a model with one single element and two nodes, one at $x = 0$ and the other at $x = L$ (illustrated in figure 3.11). The displacement of the nodes can be expressed in terms of a cubic equation [35]:

$$w(x) = A + Bx + Cx^2 + Dx^3 \tag{3.23}$$

where $w(x)$ is the vertical displacement as function of the longitudinal distance x; and A, B, C & D are unknown coefficients that must be determined from the boundary conditions at the nodes. Then, the displacement and rotation at each node are:

$$\begin{aligned} w(0) &= w_1 = A & \qquad w'(0) &= \theta_1 = B \\ w(L) &= w_2 = A + BL + CL^2 + DL^3 & \qquad w'(L) &= \theta_2 = B + 2CL + 3DL^2 \end{aligned} \tag{3.24}$$

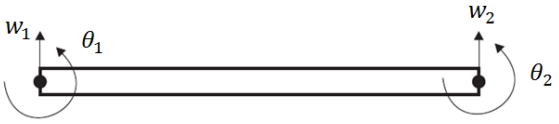

Figure 3.11: Beam element

Substituting the value of the coefficients in equation (3.23), the vertical displacement is expressed as:

$$w(x) = w_1 + \theta_1 x + \left[\frac{3}{L^2}(w_1 - w_2) + \frac{1}{L}(2\theta_1 + \theta_2)\right] + \left[\frac{2}{L^3}(w_1 - w_2) + \frac{1}{L^2}(\theta_1 + \theta_2)\right] \tag{3.25}$$

Once the vertical displacement expression has been defined, the shape function matrix $N(x)$ must be computed. The equation that relates the vertical displacement with the shape function matrix is the following:

$$w(x,t) = [N(x)]\{q(t)\} \tag{3.26}$$

where $\{q(t)\} = [w_1\ \theta_1\ w_2\ \theta_2]^T$. The shape function matrix is essential to define the mass and stiffness matrices which are required to solve the structural problem since this problem is based on one main expression:

$$[M]\,\ddot{q} + [K]\,q = R \tag{3.27}$$

where M is the mass matrix, K is the stiffness matrix and R is the generalised force vector. The mass and stiffness matrix are solved by implementing the following integrals:

$$\begin{aligned} M &= \int_0^L \rho\left(NN^T\right) dx \\ K &= \int_0^L EI\left(N''N''^T\right) dx \end{aligned} \tag{3.28}$$

Introducing the forces and the characteristics of the studied structure it is possible to solve for the displacements which is one of the principal purposes of using FEM in this assessment. In the case of static analyses, the second derivative of the displacement is 0, thus, equation (3.27) becomes:

$$[K]\,q = R \tag{3.29}$$

Furthermore, the other use of FEM is based on the normal modes of the structure. In order to get those frequencies, the eigenvalue problem of equation 3.27 is solved and the frequencies of the natural modes of the structure are computed.

3.5 Theoretical Modal Analysis

As the deflection and modal analyses of the aircraft model are performed with a finite element software, the right selection of the mesh becomes fundamental to achieve accurate results at a reasonable operational cost. Although a high number of elements result in a highly precise and accurate prediction of the modes and deflection, it considerably increases the time required by the computer to carry out the necessary mathematical operations.

A mesh sensitivity analysis is going to be performed in order to check which is the minimum number of mesh elements required to obtain acceptable results and do not barely differ conpared to those ones obtained by using more elements. When performing this analysis, the aircraft model is assumed to be compound by two types of elements: beams (fuselage, spar and joints) and plates (wing, HTP and VTP). The analysis consists of comparing the theoretical modes of a specific beam and plate with results computed by ANSYS with different number of mesh elements.

3.5.1 Beam Modal Study

The theory used to solve the theoretical modes of a beam is the Euler-Bernoulli beam due to its solving simplicity without the aid of any software.

The Euler-Bernoulli beam theory is based upon two main assumptions [29]:

- The cross section of the beam is assumed to be rigid, it does not deform (rigid-in-plane deformation). This implies neglecting the rotation of the cross section with respect to the beam axis, therefore the shear deformation produced is assumed null.
- Beam deflections are small.

Nevertheless, prior performing the analysis, a crucial fact must be taken into account: while the theoretical modes are calculated applying the Euler-Bernoulli beam theory, ANSYS software solves the modal problem using Timoshenko's beam theory. This theory differs from the Euler-Bernoulli beam in the assumption of negligible shear deformation, adding to the beam equation a shear correction which considers this deformation. In order to minimize the difference between both theories, the slender beam is modelled with a length much larger than the sides of the cross section making the shear contribution small compared with the bending of the beam.

The properties of the beam (free-free boundary conditions) to be studied are included in table 3.4:

ρ	2700 kg/m^3
E	69.5×10^9 Pa
$A(x)$	11.84×10^{-4} m^2
$I(x)$	4.37×10^{-6} m^4
ν	0.33
γ	6.62×10^{-6} m^4
G	$2.61 \times 10^{10} Pa$
J	8.73×10^{-6} m^4
l	25 m

Table 3.4: Beam properties

where:

$$G = \frac{E}{2(1+\nu)}$$
$$\gamma = t\left(w - \frac{t}{2}\right)^3 \tag{3.30}$$
$$J = 2I(x) \longrightarrow \text{Due to symmetry of the section}$$

3.5.1.1 Flexural Vibration of a Beam

Consider a beam of length l and x corresponds with its longitudinal axis so that $x = 0$ and $x = l$ are the limits of the beam. Assuming only flexural motion of the beam and free response, the equation that represents such motion is the following [6]:

$$\rho A(x)\frac{\partial^2}{\partial t^2}w(x,t) = -\frac{\partial^2}{\partial x^2}\left(EI(x)\frac{\partial^2}{\partial x^2}w(x,t)\right) \tag{3.31}$$

where $w(x,t)$ is the perpendicular displacement of the beam as a function of location and time.

As the cross section remains constant along the entire length of the beam, so do the area and the inertia moment. Then, the previous equation can be simplified to:

$$\frac{\partial^2}{\partial t^2}w(x,t) + \frac{EI}{\rho A}\frac{\partial^4}{\partial x^4}w(x,t) = 0 \tag{3.32}$$

The PDE is solved by applying the method of separation of variables. This implies that the displacement has the following form:

$$w(x,t) = X(x)T(t) \tag{3.33}$$

Substituting equation (3.33) in (3.32), the resultant expression is:

$$X(x)\ddot{T}(t) + \frac{EI}{\rho A}T(t)X^{IV}(x) = 0 \tag{3.34}$$

Which, in order to obtain a non-trivial solution, is expressed as:

$$\frac{\ddot{T}(t)}{T(t)}\frac{\rho A}{EI} = -\frac{X^{IV}(x)}{X(x)} = -\beta^4 \tag{3.35}$$

where β is an specific parameter that must be obtained to compute the bending frequencies of the beam.

Now, we will focus on the x-dependant part of the equation. This can be expressed as a 4^{th} degree ordinary differential equation (ODE):

$$X^{IV}(x) - \beta^4 X(x) = 0 \tag{3.36}$$

The solution of this ODE is the following:

$$X(x) = Asin(\beta x) + Bcos(\beta x) + Csinh(\beta x) + Dcosh(\beta x) \tag{3.37}$$

Assuming a free-free beam, the corresponding boundary conditions are:

$$\begin{cases} \partial_{xx}w(0,t) = 0 & \partial_{xxx}w(0,t) = 0 \\ \partial_{xx}w(l,t) = 0 & \partial_{xxx}w(l,t) = 0 \end{cases}$$

By applying those boundary conditions to equation (3.37), the ensuing system of equations is obtained:

$$\begin{cases} -B + D = 0 \\ -A + C = 0 \\ -Asin(\beta l) - Bcos(\beta l) + Csinh(\beta l) + Dcosh(\beta l) = 0 \\ -Acos(\beta l) + Bsin(\beta l) + Ccosh(\beta l) + Dsinh(\beta l) = 0 \end{cases}$$

which can be simplified to:

$$\begin{bmatrix} sinh(\beta l) - sin(\beta l) & cosh(\beta l) - cos(\beta l) \\ cosh(\beta l) - cos(\beta l) & sinh(\beta l) + sin(\beta l) \end{bmatrix} \begin{bmatrix} A \\ B \end{bmatrix} = 0 \tag{3.38}$$

The solution of the system of equations becomes a simple expression:

$$cos(\beta l)cosh(\beta l) = 1 \tag{3.39}$$

The first solutions for previous equation are gathered in the table 3.5:

n	$\beta_n l$
1	4.7300
2	7.8532
3	10.9956
4	14.1371
5	17.2787

Table 3.5: Equation solutions

In order to obtain the frequency corresponding to the flexural modes of the beam, we must now look at equation (3.35) and focus on the time-dependant part:

$$\ddot{T}(t) + \beta^4 \frac{EI}{\rho A} T(t) = 0 \tag{3.40}$$

The time-dependant ODE is a 2^{nd} order differential equation which has the next solution:

$$T_n(t) = A_n sin(w_n t) + B_n cos(w_n t) \tag{3.41}$$

where w_n is the natural frequency corresponding with each of the flexural modes of the system. Thus, the natural frequency can be expressed as:

$$f_n = \frac{1}{2\pi}\sqrt{\frac{EI}{\rho A}}\beta_n^2 = \frac{1}{2\pi}\sqrt{\frac{EI}{\rho A}}\left(\frac{\beta_n l}{l}\right)^2 \quad for \quad n = 1, 2, 3... \tag{3.42}$$

3.5.1.2 Torsional Vibration of a Beam

Considering the same beam as the one before, the equation which represents its torsional motion is [6]:

$$\frac{\partial^2}{\partial t^2}\theta(x,t) = \frac{G\gamma}{\rho J}\frac{\partial^2}{\partial x^2}\theta(x,t) \tag{3.43}$$

where $\theta(x,t)$ corresponds to the angle of torsion at each section of the beam and at each instant.

In this case, the method of separation of variables will be used also to solve the previous PDE, so that the angle of torsion can be expressed as:

$$\theta(x,t) = \Theta(x)T(t) \tag{3.44}$$

Plugging equation (3.44) into (3.43) and applying the same reasoning that was explained in the flexural vibrations analysis, the equation becomes:

$$\Theta(x)\ddot{T}(t) - \frac{G\gamma}{\rho J}\Theta''(x)T(t) = 0 \longrightarrow \frac{\ddot{T}(t)}{T(t)}\frac{\rho J}{G\gamma} = \frac{\Theta''(x)}{\Theta(x)} = -\lambda^2 \tag{3.45}$$

From this equation, the x-dependant part is studied:

$$\Theta''(x) + \lambda^2\Theta(x) = 0 \tag{3.46}$$

Comparing with the flexural vibrations case, the main difference between both processes is the order of the ODE, which in this case is of 2^{nd} order. The solution of such 2^{nd} order ODE is the following:

$$\Theta(x) = Asin(\lambda x) + Bcos(\lambda x) \tag{3.47}$$

As the equation is a 2^{nd} order ODE, only 2 boundary conditions for the free-free beam are required (no torque at both ends):

$$\begin{cases} \partial_x\theta(0,t) = 0 \\ \partial_x\theta(l,t) = 0 \end{cases} \longrightarrow \begin{array}{c} A = 0 \\ Bsin(\lambda l) = 0 \end{array}$$

The solution of this system of equations can be obtained straightaway unlike in the previous case, giving as result a simpler expression:

$$\lambda = \frac{n\pi}{l} \tag{3.48}$$

To compute the natural frequencies it is neccessary to study now the time-dependant part of the equation (3.45):

$$\ddot{T}_n(t) + \lambda^2\frac{G\gamma}{\rho J}T(t) = 0 \tag{3.49}$$

The time-dependant ODE is similar than the one of the flexural vibration, therefore the solution will be the same as equation (3.40). However, the natural frequency has a different expression:

$$f_n = \frac{n}{2l}\sqrt{\frac{G\gamma}{\rho J}} \quad for \quad n = 1, 2, 3... \tag{3.50}$$

3.5.1.3 Axial Vibration of a Beam

Lastly, still considering the same beam used in the previous cases, the axial vibration frequencies are to be computed. The equation that governs the free response of the axial motion of the beam is [6]:

$$\rho A(x)\frac{\partial^2}{\partial t^2}u(x,t) = \frac{\partial}{\partial x}\left(EA(x)\frac{\partial}{\partial x}u(x,t)\right) \tag{3.51}$$

where $u(x,t)$ is the displacement along the longitudinal axis of the beam.

As it happened in the flexural modal analysis, this equation can be simplified since the cross section area is constant along the beam:

$$\frac{\partial^2}{\partial t^2}u(x,t) = \frac{E}{\rho}\frac{\partial^2}{\partial x^2}u(x,t) \tag{3.52}$$

The PDE can still be solved by means of separation of variables:

$$u(x,t) = X(x)T(t) \tag{3.53}$$

which, substituting in equation (3.51) gives:

$$X(x)\ddot{T}(t) - \frac{E}{\rho}X''(x)T(t) = 0 \;\longrightarrow\; \frac{\rho}{E}\frac{\ddot{T}(t)}{T(t)} = \frac{X''(x)}{X(x)} = -\sigma^2 \tag{3.54}$$

By realizing that the ODE has the same format to the one solved in the torsional modes analysis, the final expression of the natural frequency will be equivalent to equation (3.50) but changing the constants inside the square root:

$$f_n = \frac{n}{2l}\sqrt{\frac{E}{\rho}} \tag{3.55}$$

3.5.1.4 Results

The results for some of the main elastic modes obtained previously are compared with those computed by means of ANSYS FEM in table 3.6. Different number of mesh elements are used to know which is the minimum quantity of elements that reduce the computational cost but give quite accurate results. The resultant frequencies are contained in table 3.6.

Modes	**FEM Frequencies [Hz]** Number of elements				**Theoretical Frequencies**
	200	400	800	2000	**[Hz]**
1^{st} Bending Mode	1.752	1.747	1.746	1.746	1.755
2^{nd} Bending Mode	4.867	4.819	4.811	4.810	4.839
3^{rd} Bending Mode	9.662	9.458	9.423	9.419	9.486
1^{st} Torsion Mode	56.762	56.762	56.762	56.762	54.152
2^{nd} Torsion Mode	113.470	113.470	113.470	113.470	108.303
1^{st} Axial Mode	101.470	101.470	101.470	101.470	101.471
2^{nd} Axial Mode	202.940	202.940	202.940	202.940	202.941

Table 3.6: Mesh sensitivity analysis for a solid element

The axial mode frequencies computed with ANSYS are almost identical to those obtained by means of Euler's beam theory with no dependance on the quantity of mesh elements. On the other hand, the torsion mode frequencies computed with ANSYS are similar but not equal to those coming from the theory no matter the number of mesh elements, a fact with two possible explanations: ANSYS uses Timoshenko's beam theory (as it was explained previously) or, as the procedure followed was to use a solid element in ANSYS instead of the beam element (the aircraft model will be designed with solid elements), some contribution from solid characteristics may be altering the results compared with the theory.

As both axial and torsion mode frequencies do not show any dependance with the quality of the mesh, the sentivity analysis is performed comparing the bending mode frequencies. On a first approach, the differences between frequencies are not significant except for the third bending mode using 200 elements which has a 1.85% error, reason to exclude the use of this number of elements. On the other hand, as it was seen with the torsion modes, the aim should not be solely to reach the theoretical value but to accept a similar result together with an adequate convergence. Results are similar but convergence seems to appear when using 800 elements or more. Due to that, 800 elements will compose the mesh of those parts of the model that have beam characteristics.

3.5.2 Plate Modal Analysis

Once the optimum panels distributions for the wing and HTP aerodynamic analysis have been obtained, the structural mesh must be studied in order to couple the best option which allows to get accurate results in both structural and aerodynamic analyses without incrementing significantly the computational cost. The plate studied here has all the edges simple supported and the physical characteristics are included in table 3.7.

ρ	2700 kg/m^3
E	70.0×10^9 Pa
$A(x)$	ab
t	0.001 m
ν	0.33
D	6.546 Pa· m^3
a $(wing/HTP)$	200/60 cm
b $(wing/HTP)$	25/20 cm

Table 3.7: Plate properties

where a is the long side of the plate, b is the short side of the plate and D is expressed as:

$$D = \frac{Et^3}{12(1-\nu^2)} \tag{3.56}$$

To compute the theoretical modes of the plate, the classical plate theory is applied [24]. The fundamental equation of the classical plate theory is:

$$D\nabla^4 w = -\rho t \frac{\partial^2 w}{\partial t^2} \tag{3.57}$$

in which w is the vertical displacement and $\nabla^4 = \nabla^2\nabla^2$, being ∇^2 the Laplacian operator so that:

$$\nabla^2 = \frac{\partial^2}{\partial x^2} + \frac{\partial^2}{\partial y^2}$$

As the free response of the plate is being studied, the vertical displacement can be expressed as:

$$w(x,y,t) = W(x,y)cos(\omega t) \longrightarrow W(x,y) = X(x)Y(y) \tag{3.58}$$

where $X(x)$ and $Y(y)$ are the mode shapes of the plate. Plugging this equation into equation (3.57), the resulting expression is:

$$\left(\nabla^4 - \frac{\rho t \omega^2}{D}\right) W = 0 \tag{3.59}$$

The boundary conditions of a simple supported plate are the following:

$$\begin{cases} w(x=0,a) = 0 & M_x(x=0,a) = 0 \\ w(y=0,b) = 0 & M_y(y=0,b) = 0 \end{cases}$$

From the boundary conditions, the solution that fulfils them is:

$$W(x,y) = A_{nm} sin\left(\frac{m\pi x}{a}\right) sin\left(\frac{n\pi y}{b}\right) \tag{3.60}$$

Substituting into equation (3.59), the natural frequencies of the simple supported plate are given by:

$$f_n = \frac{1}{2\pi}\sqrt{\frac{D}{\rho t}}\left[\left(\frac{m\pi}{a}\right)^2 + \left(\frac{n\pi}{b}\right)^2\right] \tag{3.61}$$

3.5.2.1 Results

Following a similar procedure than for the beam analysis, the first 6 theoretical bending modes of the plate will be compared with different mesh distributions (for both wing and HTP) in order to reach to an optimal distribution that combines both accuracy and low computational cost. Table 3.8 shows the results for the wing bending modes:

Panels (y - x)	Frequency [Hz]					
	1^{st} Mode	2^{nd} Mode	3^{rd} Mode	4^{th} Mode	5^{th} Mode	6^{th} Mode
80-10	39.742	41.565	44.606	48.866	54.349	61.056
100-10	39.742	41.567	44.610	48.873	54.358	61.067
120-10	39.742	41.567	44.610	48.873	54.358	61.067
160-10	39.742	41.567	44.610	48.873	54.358	61.067
80-16	39.742	41.570	44.618	48.887	54.378	61.093
100-16	39.742	41.570	44.618	48.887	54.378	61.093
120-16	39.742	41.570	44.618	48.887	54.378	61.093
160-16	39.742	41.570	44.618	48.887	54.378	61.093
80-20	39.742	41.571	44.619	48.888	54.380	61.095
100-20	39.742	41.571	44.619	48.888	54.380	61.095
120-20	39.742	41.571	44.619	48.888	54.380	61.095
160-20	39.742	41.571	44.619	48.888	54.380	61.095
Theoretical Modes	39.745	41.580	44.637	48.917	54.421	61.147

Table 3.8: Wing bending modes frequencies

In a first approach, there is not any mesh that gives as a result an identical value to the theoretical solution. This difference is due to the fact that a solid element is being studied in ANSYS while the theoretical modes have been obtained by applying Kirchhoff-Love thin plate theory [32]. However, as the plate is very thin, the variation in the results involve only a small percentage.

Moreover, any of the values obtained is acceptable compared with the converged value as the error is not bigger than a 0.2% for any of the panels distribution. Nevertheless, the best option is assumed to be, despite the small error, the one that provides a result which does not differ significantly from other distributions with a higher number of panels. Although the

variation is quite low in all the cases, convergence takes place using 16 panels in x-direction but being irrelevant in the result to use 80 or 160 panels in y-direction. Although the 80 x 16 distribution would give accurate results in terms of the structural analysis, in previous section it was specified that the number of panels spanwise required to obtain accurate results is 100 while the minimum number of panels chordwise was 10.

Therefore, the panels distribution chosen for the wing is 100 panels in y-direction and 16 panels in x-direction.

The frequencies for the HTP are gathered in table 3.9:

Panels (y - x)	Frequency [Hz]					
	1^{st} Mode	2^{nd} Mode	3^{rd} Mode	4^{th} Mode	5^{th} Mode	6^{th} Mode
20-10	67.896	88.197	122.090	169.660	230.910	251.390
40-10	67.897	88.191	122.080	169.570	230.670	251.390
60-10	67.897	88.191	122.080	169.570	230.660	251.390
80-10	67.897	88.191	122.080	169.570	230.660	251.390
20-16	67.904	88.224	122.120	169.680	230.890	251.310
40-16	67.906	88.219	122.120	169.630	230.730	251.320
60-16	67.906	88.219	122.120	169.630	230.730	251.320
80-16	67.906	88.219	122.120	169.630	230.730	251.320
20-20	67.904	88.226	122.120	169.680	230.870	251.310
40-20	67.906	88.221	122.130	169.630	230.740	251.310
60-20	67.906	88.221	122.130	169.630	230.730	251.310
80-20	67.906	88.221	122.130	169.630	230.740	251.310
Theoretical Modes	67.941	88.323	122.293	169.852	230.999	251.381

Table 3.9: HTP bending modes frequencies

Following the same procedure than before, although the variation of the frequency between the different distributions is small, the option that reaches the condition of convergence with the lower number of panels is 40 x 16 distribution which gives identical results to those obtained with a 80 x 20 distribution.

Comparing with the aerodynamic results, the 40 x 16 distribution has a 2.04% of error which is not adequate for the analysis, for that reason the mesh distribution selected for the HTP is 80 panels in y-direction and 16 panels in x-direction, which is the optimum combination between the aerodynamic and the structural meshes.

3.6 Fluid-Structure Coupling Methodology

The last step in the process of solving the static aeroelastic problem presented is to develop a procedure by which the fluid-structure interaction can be assessed. From the aerodynamic model, the pressure developed over the surfaces is obtained and it must be imposed into the structural model so deformations can be computed. Then, these deformations must be introduced into the aerodynamic model so the new geometry is defined and the new pressures are calculated. An iterative process is performed until convergence is achieved.

It is fundamental to recall that the angle of incidence is not the same for the wing and for the HTP. For simplicity, in order to neglect the elevators, the HTP is able to rotate around the y-axis so it can have a different angle of incidence than the wing. This section describes the methodology followed for the different analysis. The results obtained will be presented in chapter 6.

3.6.1 Cruise Configuration

The first step in the solving process is to determine the cruise conditions which are required for the gust load factor computation. Within the cruise phase, two different cases are studied: assuming that the wing and the HTP are rigid (do not present any deformation) and accounting for the flexibility of the material.

3.6.1.1 Rigid Surfaces

This is the simplest case. As the flexibility of the material is not being considered, deformations are not being produced when the loads are applied, and thus, no iterative process is needed. The fluid-structure procedure followed in this case is described below:

1. The structure implemented in the aerodynamic model is the rigid surface for the wing and HTP which are designed in chapter 5.
2. The steady cruise and longitudinal equilibrium conditions are included in the code in order to compute the lift that must be generated by each surface to fulfil the flight mechanics conditions.
3. Once the lift required and the geometry of the surface have been included, the 3D numerical panel method is executed at different angles until all conditions are met. This iteration is performed assuming linear behaviour by first computing $C_L(\alpha = 0°)$, then $C_L(\alpha = 10°)$ and last computing $dC_L/d\alpha$ so the angle of attack and the HTP angle at cruise can be obtained from the longitudinal equilibrium and lift equal weight conditions.

3.6.1.2 Flexible Surfaces

The objective in this case is the same: obtain the cruise configuration, however the process is more complex due to the inclusion of structural flexibility effects in the calculations. Because of flexibility, the surfaces are deformed when pressure is applied on them, producing a change in the geometry which, in turn, varies the pressure distribution along the surface. Thus, an iterative procedure must be defined to determine the specific values of the angle of attack and angle of the HTP at which the conditions are fulfilled and, at the same time, stabilize the deformation so there is no further change in the geometry under that configuration.

1. From the cruise configuration for the rigid surfaces, the pressure distribution is computed.
2. The pressure at each panel is exported to the corresponding mesh element in the structural module. The static structural problem is solved and the deformations at each of the nodes that constitute the surfaces are obtained.
3. The deformation is added to the rigid geometry so the new flexible geometry is defined. With the new geometry, the 3D numerical panel method is applied to get the angles that fulfil the defined conditions (this procedure is identical to the one used in the rigid structure), obtaining the new pressure distribution.
4. Repeat steps 2-5 until the angles for both wing and HTP converge.

3.6.2 Gust effect analysis

Once the cruise configurations for both cases (rigid and flexible) have been determined, the analysis of the load factor with the inclusion of a gust can be carried out. This evaluation is divided in three different cases that depend on the rigidity/flexibility assumption in both cruise and gust condition. This study, in turn, is going to be conducted twice since two alternative gust speed designs were explained previously.

3.6.2.1 Rigid Cruise-Rigid Gust

In this specific example, the surfaces are considered rigid at both phases: when flying at cruise and at the encounter of a vertical gust. Thus, there is no need of implementing an iterative process since the geometry is not going to vary no matter the magnitude of the pressure applied. The aerodynamic model implemented in this case is even simpler than for cruise condition since, now, the longitudinal equilibrium and lift equal weight conditions do not have to be fulfilled; the lift of each surface is computed by means of the effective angle of attack: $\alpha_e = \alpha_{cruise} + \Delta\alpha$. The fluid-structure methodology applied is the following:

1. Implement the geometry and angle for the rigid surfaces in cruise.
2. Compute the effective angle of attack for the two gust profiles obtained previously.
3. Compute the load factor generated with the new angle of attack by using the 3D numerical panel method.

3.6.2.2 Flexible Cruise-Rigid Gust

This is an interesting case in which, during cruise, the effect that structural flexibility has on the aerodynamic forces is included; nonetheless, when the aircraft enters into the gust, the surfaces are assumed to be rigid, they are not deformed despite the increase of the aerodynamic loads. Because of this assumption, the evaluation applying this specific condition is quite similar to the rigid cruise-rigid gust, being the geometry input the only difference:

1. Implement the geometry and angles for the flexible surfaces in cruise.
2. Compute the effective angles for the two gust profiles obtained previously.
3. Compute the load factor generated with the new angles of incidence by using the 3D numerical panel method.

3.6.2.3 Flexible Wing-Flexible Gust

In this last example, the most realistic conditions are studied. The flexibility of the material is accounted for in the two phases that are evaluated in this project. Therefore, this supposes the most complex case of this thesis since the number of iterations required to obtain the final value is quite larger than the rest of the cases: while the other two gust responses can be solved with only one execution of the aerodynamic code, this gust performance requires an iterative process since the geometry of the surfaces changes as aerodynamic loads vary.

1. Start from the end point of the flexible cruise-rigid gust case.
2. Export the pressure at each panel into the structural module.
3. Solve the static structural problem and obtain the deformations produced.
4. Add the deformations to the rigid structure in order to obtain the new deformed geometry and compute the pressure distribution for the new geometry maintaining the previous angles.
5. Repeat steps 3-4 until convergence of the load factor is achieved.

Chapter 4

Model Design

The next step is to design the whole aircraft model so the analysis can be performed. Nevertheless, instead of designing the model with the different details that constitute the structure of an aircraft, some assumptions and simplifications are considered.

4.1 Design process assumptions

The assumptions to be made are aimed to reduce the complexity and computational cost by considering that these do not affect significantly the results of the study. The main assumptions made are the following:

- **Tail Design**

One of the most important design characteristic that has been defined is the type of tail used. Two possibilities were considered: standard tail or T-tail formats (figure 4.1).

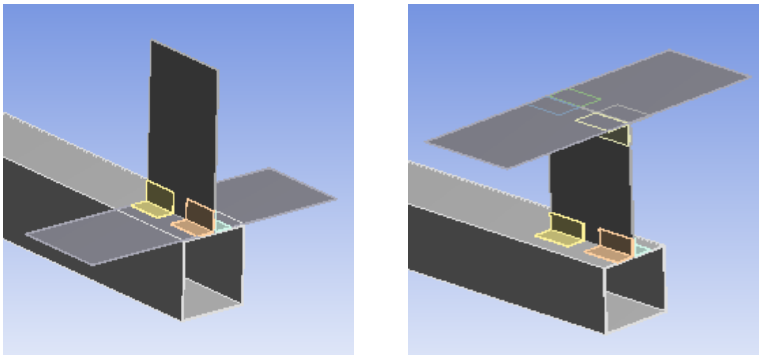

(a) Standard tail (b) T-tail

Figure 4.1: Tail design

Both configurations have their advantages and disadvantages. For example, the standard tail has the advantage that the VTP does not have to withstand the loads of the HTP, what reduces the structural requirements of the VTP. On the other hand, the T-tail model has the advantage that the air going into the HTP is clean, it is not disturbed by its way over the wing; however, such design implies that the VTP holds the HTP having to increase the strenght of the VTP and, in turn, its weight.

Despite the reduction in weight provided by the standard tail, the T-tail is chosen for this study since the aerodynamic model developed will be more adequate than using the standard tail. Designing the aircraft with a standard tail would require to model the effect of the wing's wake on the flow of the HTP, increasing significantly the complexity of the aerodynamic model.

- **HTP Design**

Another part that is interesting for the analysis is the HTP. The HTP has a contribution on the lift of the aircraft but its most important function in this assessment is to impose longitudinal equilibrium conditions. The longitudinal equilibrium of the aircraft is controlled by the elevators located at the trailing edge of the HTP. Although the inclusion of the elevator deflection in the aerodynamic model is not complex, it does add complexity to the structural model. For simplification, the HTP is going to be assumed as a flat plate which can rotate around y-axis, so it can face a different angle of incidence than the wing, producing the same lift that if it had elevators. The equivalence with the real HTP model is represented in the following equation:

$$C_L(\alpha_{HTP}) = C_L(\alpha) + C_L(\delta_e) \tag{4.1}$$

- **Exposed Wing**

In actual aircraft the wing is attached at the fuselage by means of belly fairings. Thus, there is a section of the wing that does not produce any lift since it is joined to the fuselage. The whole wing, adding the part attached to the fuselage, is called reference wing, while the surface of the wing that is producing lift is called exposed wing.

In the analysis, the exposed wing is going to be assumed equal to the reference wing, i.e, the pressures obtained from the aerodynamic calculations that correspond to the wing section covered by the fuselage are going to be applied as if the fuselage was not there.

- **Parts connections**

The aircraft model that is intended to be built is composed of plates and aluminium profiles which must be joined together. The method to establish the connections can be either by means of bolts or welding.

At first, in the FEM model the connections are going to be assumed infinitely rigid. However, in the future, the modal frequencies obtained in the FEM model will be compared with the experimental ones (once the model is manufactured). With this comparison the model will be updated if needed.

4.2 Model Geometric Dimensioning

The model of the aircraft must be designed with all the parts necessary to represent properly the structural features of a real aircraft. This model is intended to be similar to an actual aircraft in regard of the structural characteristics. In order to achieve the desired similarity, the aircraft is designed following two main ideas: to define the dimensions of the model to be smaller (2m. span) but proportional to the C-295; and to modify the thickness and dimensions[1] to obtain similar modal frequencies than a real aircraft.

Nevertheless, the modal frequencies of real aircrafts as the C-295 are confidential and not possible to find. For this reason, the modal frequencies are compared with those presented by papers [23] & [34], who also design aircraft models that are not real. Another drawback found is the complexity to design a specimen whose natural frequencies match those coming from the references; then, to obtain a 'valid' model, only three frequencies of the principal parts studied (wing & tail) must agree in order of magnitude with those obtained from the references.

The principal aeroelastic modal frequencies for the final model are gathered and compared with those of the references:

Modes	***Modal Frequencies [Hz]***		
	Model	**Reference [23]**	**Reference [34]**
1^{st} symmetric wing bending	7.9675	8.1913	8.815
1^{st} VTP bending	9.7681	9.8644	9.513
1^{st} asymmetric wing bending	15.804	-	-
1^{st} symmetric wing torsion	17.790	31.085	30.48
2^{nd} asymmetric wing bending	19.476	29.331	31.63
1^{st} symmetric HTP bending	20.291	21.219	13.605
1^{st} VTP torsion	21.614	16.179	96.38

Table 4.1: Aircraft aeroelastic modes

[1] Feasible dimensions and thickness obtained from Alu-Stock catalogue: `http://www.alu-stock.es/`

Data contained in table 4.1 show a certain similarity between the modal frequencies for some specific modes. For example, in relation to reference [23], there is proximity in the values for 1^{st} symmetric bending for wing, VTP and HTP while there is an important difference in the 1^{st} symmetric wing torsion and 2^{nd} asymmetric wing bending. These two last modes are very alike among the references; nevertheless, the difference between our model and the references is not considered as an error because some aspects as spar position influence the modal frequencies of the wing. The authors of the references design models following distinct approaches: addition of ribs and a rear spar to increase the stiffness of the surfaces, which can explain the contrast between frequencies. The design performed in this work wanted to keep the structure as simple as possible to allow manufacturing the model in the University facilities.

On the other hand, a significant difference regarding the 1^{st} symmetric HTP bending and 1^{st} VTP torsion is found for reference [34]. Aside from the addition of ribs and rear spar, the tail from reference [34] is based on the standard configuration while the tail from reference [23] is a T-tail design. The decrease on the weight of the VTP which does not hold the HTP in the standard tail may explain that these modes show a substantial variation in frequencies compared to the designed model and reference [23].

The agreement between the modal frequencies of some principal modes of the aircraft is achieved by an iterative process in which thickness and dimensions of the aircraft parts are simulated until a similarity between modes is obtained. A global picture of the model with the names that have been assigned to the parts is presented in figure 4.2:

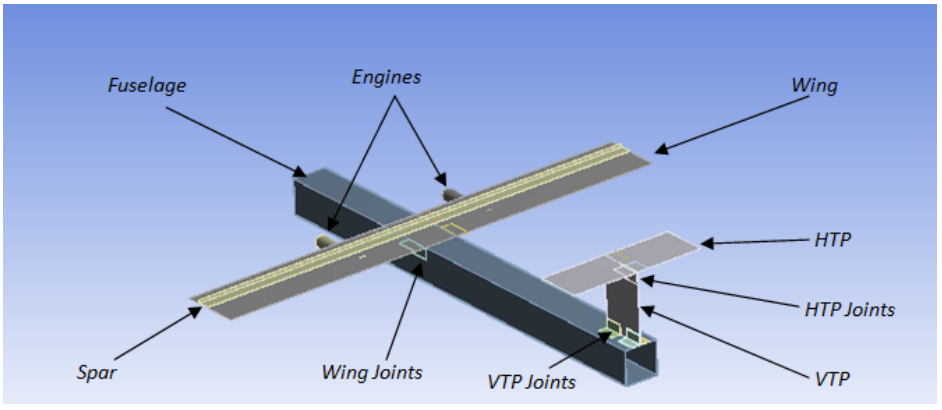

Figure 4.2: Model parts

The thickness and material selected for each part are included in table 4.2 and the dimensions are presented on the draft (made with Solid Edge [31]) located within appendix A.

Part	Thickness [mm]	Material
Fuselage	3.0	Aluminium 6063
Wing	1.0	Aluminium 6082
VTP	3.0	Aluminium 6082
HTP	1.5	Aluminium 6082
Spar	2.0	Aluminium 6063
Engines	2.5	Aluminium 6063
Wing joints	2.0	Aluminium 6063
VTP joints	2.0	Aluminium 6063
HTP joints	2.0	Aluminium 6063

Table 4.2: Thickness & material

4.3 Wing Configurations

The model designed is studied by setting different configurations to achieve a layout that provides gust load alleviation compared to the rigid structure assumption. These configurations are based on a standard specimen and two other designs that modify the aerodynamic and structural characteristics.

4.3.1 Standard Design

The aerodynamic characteristics of this model correspond to the specimen designed in previous section, the airfoil profile is assumed to be symmetric since the wing and HTP of the experimental model are made of plates.

On the other hand, the spar, which determines the elastic properties of the wing (besides the material of the plate), is located in the usual position of 25% the chord of the wing, placing the elastic axis at 26% of the chord. Hence, the center of mass of the wing will be located at 44% of the chord.

Due to the results obtained in section 5.1 (there is no load alleviation due to structural flexibility), two more configurations are approached in a bid to achieve load alleviation.

4.3.2 Aerodynamic Modification

In this case, the design maintains the position of the spar as in the standard design. However, the airfoil profile is changed in the aerodynamic model from a symmetric profile to a cambered one. Specifically, the airfoil profile used is the NACA 2410. The reason is that this modification allows to move rearwards the center of pressure of the wing, trying to locate it behind the elastic axis.

4.3.3 Structural Modification

The last modification consists of, maintaining the aerodynamic profile symmetric, the spar is moved forward. Instead of moving the center of pressure behind the elastic axis, the elastic axis is moved to locate it ahead the center pressure. In order to achieve so, the spar is placed at the leading edge of the wing, positioning the elastic axis at the 3% of the chord and center of mass of the wing at the 36% of the chord.

Evaluating the effect of structural flexibility with the designs mentioned above will allow to compare the different configurations and how to achieve load alleviation, which, if achieved, could lead to a significant reduction of aircraft weight and costs.

Chapter 5

Results & Discussion

The explained analysis is performed on the designed model in two conditions: cruise and vertical gust encounter. The model is evaluated in three distinct configurations and with two different vertical gusts which correspond to each of the certification approaches assumed (CS-25 giving $\Delta\alpha = 7.060°$ and CS-VLA giving $\Delta\alpha = 20.857°$). The effect of structural flexibility on the load factor will be discussed for each of the configurations by comparing the loads produced on the flexible structure with those generated on the rigid one.

Along the evaluation of the results, three main locations of the wing are going to be referred to explain the effect of structural flexibility:

- The center of pressure of the wing, computed using equation 3.3.
- The center of mass of the wing, which is the point where the weight and g-forces are applied.
- The elastic axis of the wing.

These locations are going to be referred to their position along the chord, their situation regarding the spanwise direction is not considered in the assessment.

5.1 Standard Design Analysis

The first study performed is the one corresponding to the standard design, the model that best represents the aircraft evaluated: elastic axis at the 26% of the wing chord and symmetric airfoil since the wing of the model is made of a flat plate. In turn, the analysis is divided in two main sections: cruise phase and vertical gust encounter.

5.1.1 Cruise Analysis

Prior to study the response of the aircraft to an uniform vertical gust, the initial conditions of the aircraft must be set. These initial conditions of an aircraft correspond to the steady cruise flight at longitudinal equilibrium, thus, an evaluation of the configuration (angle of attack and HTP angle) that must be set to achieve such conditions is carried out for both rigid and flexible structure.

Cruise Results	$\alpha_{\mathbf{wing}} = [^\circ]$	$\alpha_{\mathbf{HTP}} = [^\circ]$
Rigid Structure	2.2803	6.5913
Flexible Structure	1.8870	6.2938

Table 5.1: Cruise analysis for the standard design

Given the data contained in table 5.1, it is noticeable that the required angle of attack to maintain cruise is lower for the flexible structure than for the rigid one. This implies that the flexible surfaces produce more lift than when assuming rigid structure. Such aspect can be explained with the twist developed by the aerodynamic forces in the wing.

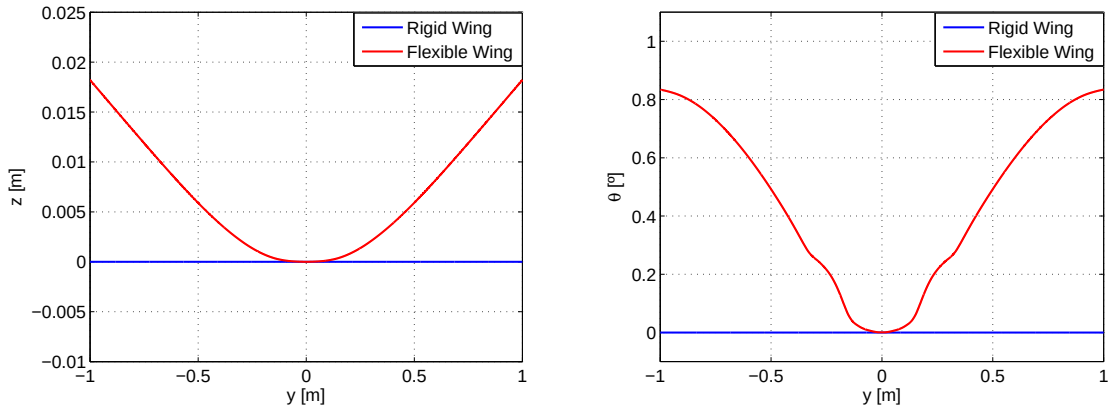

(a) Vertical displacement along the span

(b) Twist along the span

Figure 5.1: Elastic deformation of the wing at cruise

First, note that the section's vertical displacement shown coincides with the elastic axis of the wing since the contribution of twist to the vertical distance at that location is null. Then, figure 5.1(a) shows that, except for the center of the wing (which is the part attached to the fuselage), the bending of the wing follows a nearly-linear trend. It is noticeable that the vertical displacement is quite small compared with the span, so the dihedral effect that structural flexibility induces on the wing might be considered negligible as the dihedral angle generated is about 1°.

On the other hand, as the bending produced by aerodynamic loads does not have a significant effect on the aerodynamics of the wing, elastic twist would be the other parameter that makes different the cruise requirements for rigid and flexible structures. Figure 5.1(b) reveals a positive induced twist (nose-up), whose formation was explained in the introduction but will be corroborated with the lift distribution along the chord. The nose-up twist has a significant effect on aerodynamics as it is up to a 36% of the angle required for cruise with a rigid wing. As it is a nose-up twist, the effective local angle at each section of the wing is greater than the actual angle of attack, justifying that the angle of attack must be lower for the flexible wing than for the rigid wing (the same happens for the HTP).

However, two remarkable parts of the twist distribution must be studied. The first one is the sudden change on the trend that takes place around 0.3-0.4 m. from the center of the wing. This steep variation occurs because of the engines, which are located at 0.3 m. from the middle of the wing. As the engines are attached at the front part of the wing, their weight pulls down the front of the wing where they are located, decreasing the twist induced at this section. The other significant aspect is the behaviour of the twist as it gets closer to the wingtip. As the sections of the wing get closer to the tip, the twist growth diminishes. This trend can be explained with the distribution of lift along the span.

Figures 5.2(a) & 5.2(b) represent the sum, spanwise and chordwise, of the lift generated at each section.

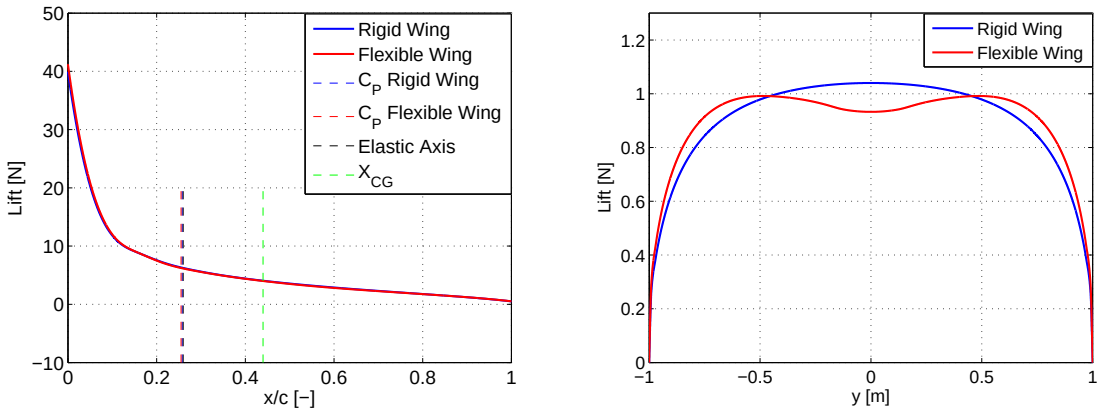

(a) Lift distribution over the chord

(b) Lift distribution over the span

Figure 5.2: Lift distribution over the wing at cruise

Starting with the lift distribution over the chord, remark that the lift distributions are quite similar for rigid and flexible wings, having the center of pressure located in the same place. Nevertheless, it must be explained that the nose-up twist mentioned before is produced mainly by the weight of the wing not by the aerodynamic load because the elastic axis is almost coincident with the center of pressure.

Furthermore, regarding the lift distribution over the span, the differences are more evident. A lift redistribution takes place when flexibility is taken into account. The lift at the center of the wing (part attached to the fuselage) is lower because the angle of incidence is smaller and because this part does not have any twist. Hence, the lift distributes depending on the effective angle of each section; a similar trend can be observed in [27], where the flexible wing shows an increased lift along the chord compared to the rigid wing. The other noticeable aspect is that the lift does not suffer an instantaneous drop at the tips of the wing but this drop starts in the inner part of the wing, being more pronounced at the edges. This drop is produced due to the wingtip vortices which reduce the lift generated as the section is closer to the tip. As lift is lower the closer to the tip, the torsion moment generated at the elastic axis decreases and so does twist. This is because the lift decreases and the contribution of the aerodynamic loads becomes even smaller. That is why the twist does not grow linearly in sections close to the tip, in fact, it seems to remain nearly constant (Figure 5.2(b))

5.1.2 Vertical Gust Analysis

After setting the configuration to maintain cruise flight with longitudinal equilibrium, it is possible to study the structural response to entering into a uniform vertical gust. The response to both of the gust profiles is evaluated for 3 different assumptions: the structure is assumed rigid for cruise and gust phases (RR), the structure is assumed flexible for cruise but it does not deform when the aerodynamic loads are increased due to the gust (FR), and the flexibility of the aircraft is accounted for both flight conditions (FF).

The main variables analysed during the encounter with the vertical gust are the variation in lift corresponding to the wing and the HTP, the load factor and the reduction in load factor in relation to the RR case (load factor alleviation). These variables are gathered in table 5.2.

$$N_z = \frac{\Delta L}{W} + 1 \tag{5.1}$$

	$\boldsymbol{\Delta\alpha = 7.060°}$			$\boldsymbol{\Delta\alpha = 20.857°}$		
	RR	FR	FF	RR	FR	FF
ΔL_{wing} $[N]$	278.61	278.45	326.07	798.54	797.56	905.38
ΔL_{HTP} $[N]$	46.00	45.94	47.47	129.09	128.85	131.61
Load factor (N_z)	3.442	3.440	3.810	7.978	7.969	8.800
Load factor alleviation (%)	-	0.05	-10.69	-	0.12	-10.31

Table 5.2: Gust encounter analysis for the standard design

From the table, the first outstanding aspect that can be observed is that the load factor at the FR assumption does not almost vary when compared to the RR case. Nevertheless, the

result agrees with what it was expected as the variation of lift with the angle of attack is equal; or almost identical, for both.

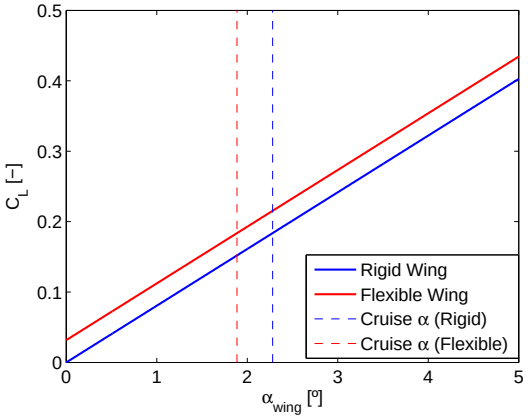

Figure 5.3: $C_{L,wing}$ vs. α_{wing} for the standard design

Figure 5.3 illustrates the lift coefficient as a function of the angle of attack for the rigid and deformed wings. This plot shows that the elastic twist produced by the aerodynamic loads reduces the angle of attack of zero-lift but it does not vary the slope of the lift coefficient with regard to the angle of attack, having the same variation of lift at a given gust profile.

On the other hand, when considering the aircraft flexible in both cruise and gust encounter, the load factor increases significantly as compared to the rigid structure assumption. This increment depends on the rise of the twist produced by the aerodynamic loads.

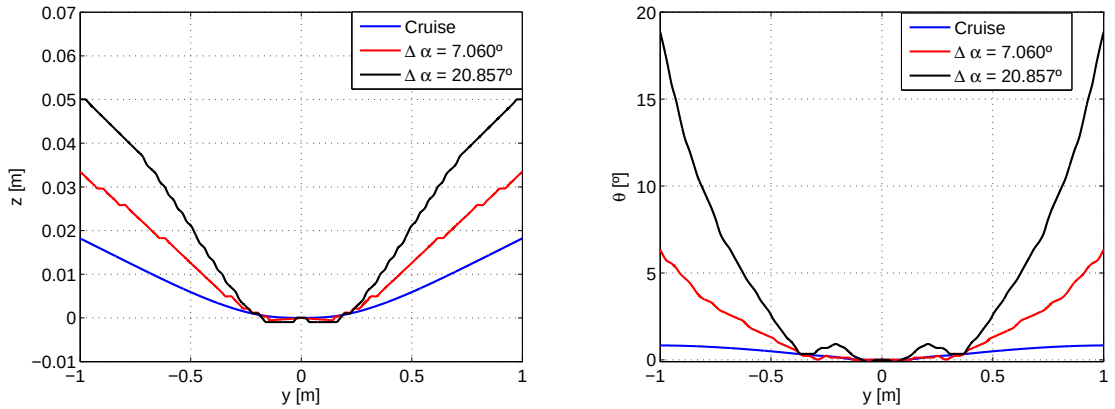

(a) Vertical displacement along the span

(b) Twist along the span

Figure 5.4: Elastic deformation of the wing with vertical gust

The bending of the wing, as expected, increases as the angle of attack rises. Nevertheless, the contribution of the dihedral is still very low as the dihedral angles that are produced by

the gust increments of 7.060° and 20.857° are 1.8° and 2.9°, respectively, which imply that most of the normal force to the wing is contributing to lift instead of lateral force.

On the contrary, the elastic twist increases greatly, having a huge impact on the aerodynamic forces. For both gust profiles, the twist angle increases significantly the effective local angle of incidence, which, in turn, has a detrimental effect on the load factor, rising it up to more than a 10% for both gust profiles. Figure 5.4 shows the benefitial effect of the engines located forward of the wing on the elastic twist by reducing it. As opposed to what it happened for cruise, the twist for both gust profiles keeps growing (even at a higher rate) in regions near the tips. For better explanation, this analysis is performed using the pressure distribution introduced by figure 5.5.

It seems evident that, although wing bending has an alleviating effect on the load factor, this is not enough to counteract the increase of lift produced by the additional twist generated by the external loads. Also, it is important to study the effect of flexibility on the stresses at the root, which can be deduced from the lift distribution along the span.

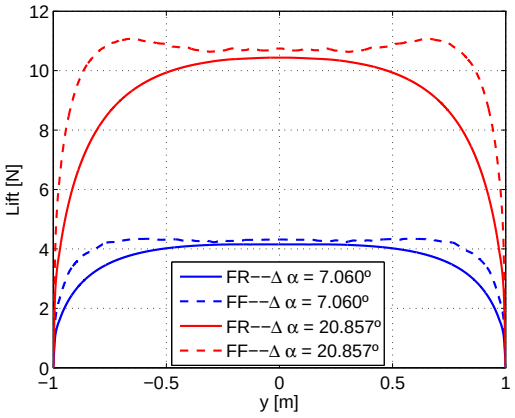

Figure 5.5: Lift distribution over the chord with a vertical gust

The shear stress at the root is directly proportional to the load factor, as greater is the lift produced, larger is the shear stress at the root. Then, as the flexible wing has a larger load factor than the rigid one, it seems clear that the shear stress at the root will be larger. On the other hand, the bending moment at the root is easily explained with the lift distribution over the span. Previously, at the cruise phase, it was obtained that the flexible wing produced larger bending moments at the root than the rigid wing because of the change on the lift distribution over the span. In the case of encountering a gust the result is not different, figure 5.5 proves that the lift is larger in the outer part of the wing than in the inner part in comparison with the rigid structure. This produces a larger bending moment at the root that must be taken into account in the design of the aircraft.

Regarding the relation between previous twist trend and the pressure distribution over the span, the reason for the twist to increase at a higher rate is due to the increase in lift in the middle-outer section of the wing. As well, although the lift decreases to zero at the tips, such drop is faster than in cruise conditions and does not allow any margin to slow the growth of the twist.

The main option to achieve load alleviation is to develop a nose-down twist as in [16], who include a separate wing segment at the tip that generates a nose-down twist when the aircraft encounters a gust. Unlike [16], the method implemented to induce a nose-down twist is to benefit from the structural flexibility of the wing by locating the center of pressure after the elastic axis and to position the center of mass near the elastic axis, thus, decreasing the effective angle of attack.

5.2 Aerodynamic Modified Design

By evaluating the standard design, the main conclusion obtained was that, in order to achieve load alleviation, the center of pressure must be located after the elastic axis so a nose-down torsion moment is produced on the elastic axis. The first approach to achieve this goal is to change the airfoil implemented in the wing and HTP. Cambered airfoils do not only produce more lift than a symmetric one for a given angle of attack, but also redistribute the lift along the chord. For this reason, the analysis is repeated as before but using in this case the NACA 2410 instead of a symmetric airfoil.

5.2.1 Cruise Analysis

The same procedure is followed, so the cruise angles at which the aircraft is flying are obtained assuming rigid and flexible lifting surfaces.

Cruise Results	$\alpha_{\mathbf{wing}} = [^\circ]$	$\alpha_{\mathbf{HTP}} = [^\circ]$
Rigid Structure	0.4123	3.4955
Flexible Structure	2.1450	3.3629

Table 5.3: Cruise analysis for the aerodynamic modified design

Significant differences in contrast to the standard design already appear in the cruise phase. First, the angles contained in table 5.3 for the rigid structure are much lower using a cambered airfoil, as it was expected. However, concerning the flexibility of the aircraft, the angles of the flexible aircraft increase when compared to the rigid assumption, unlike it happened for the standard design.

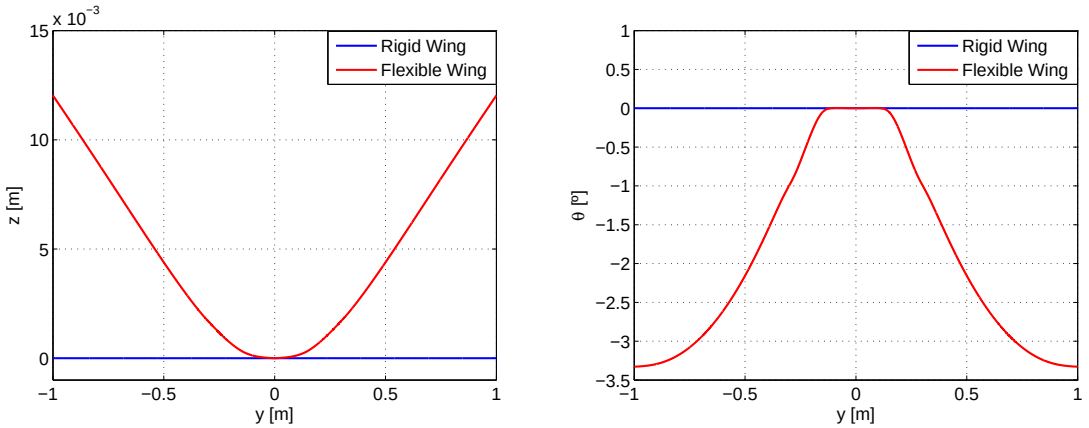

(a) Vertical displacement along the span

(b) Twist along the span

Figure 5.6: Elastic deformation of the wing at cruise

Figure 5.6(a) shows that wing bending is quite similar to the one corresponding to the standard design in order of magnitude and trend. However, the twist (shown in figure 5.6(b)) for this case turns out to be negative (nose-down), which leads us to believe that load alleviation in the encounter of a vertical gust can be achieved using cambered profiles. The lift distribution over the wing is studied in figures 5.7(a) & 5.7(b) to verify that the position of the center of pressure is the cause of the nose-down elastic twist.

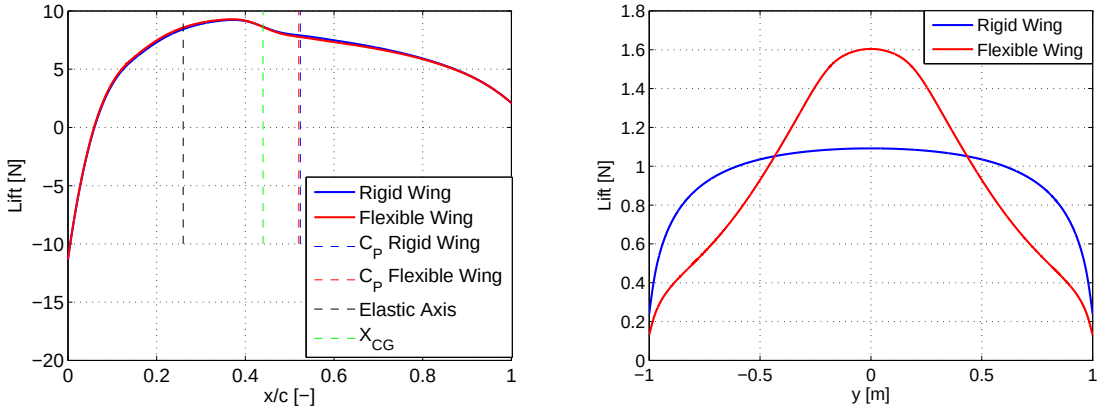

(a) Lift distribution over the chord

(b) Lift distribution over the span

Figure 5.7: Lift distribution over the wing at cruise

Regarding the lift distribution along the chord, the most important aspect that appears is that the center of pressure is located after the elastic axis as it was intended, producing the nose-down twist seen on figure 5.6(b). This relocation of the center of pressure is due to the more uniform lift distribution and the negative peak that appears at the leading edge, while the symmetric airfoil showed a large positive peak at the leading edge. Despite the center of

pressure is after the elastic axis, so does the center of gravity which has the opposite effect. Nonetheless, there are two reasons that explain the greater relevance that the aerodynamic load has in this case: first, the distance between the center of pressure and the elastic axis is larger than the distance from the center of gravity to the elastic axis, therefore the torsion produced by the lift is larger; secondly, the aerodynamic load is equal to the total weight of the aircraft while the percentage of weight that is affecting the torsion of the wing is the one corresponding to the spar and wing weights, a 15% of the total mass of the aircraft.

The lift distribution over the span shows a significant difference in comparison with the standard design results. In this case, most of the lift is produced in the inner part of the wing. Whereas this does not have any effect on the shear stress at the root (same lift for rigid and flexible wings), it does produce an important benefitial effect reducing bending moment at the root. Because of this, the standard design has a wing that has a higher dihedral angle (produced by the bending of the wing) than this case.

5.2.2 Vertical Gust Analysis

Although the results obtained at cruise give rise to the thought that the flexibility of the structure has an alleviation effect on the load factor and stresses at the root when it comes to encountering a gust, the analysis must be performed to support such conclusion. Relevant data concerning this case is enclosed in table 5.4.

	$\mathbf{\Delta\alpha = 7.060^\circ}$			$\mathbf{\Delta\alpha = 20.857^\circ}$		
	RR	FR	FF	RR	FR	FF
ΔL_{wing} $[N]$	278.61	282.45	322.81	803.95	818.95	921.65
ΔL_{HTP} $[N]$	46.00	46.24	47.67	131.17	131.16	133.14
Load factor (N_z)	3.442	3.472	3.787	8.034	8.147	8.934
Load factor alleviation (%)	-	-0.89	-10.03	-	-1.40	-11.20

Table 5.4: Gust encounter analysis for the aerodynamic modified design

In this case, as it happened with the standard design, there is not alleviation of the load factor when encountering a vertical gust. Although the center of pressure has been moved after the elastic axis, the aerodynamic loads keep being greater for the flexible aircraft than for the rigid one. Such effect might mean that the elastic twist becomes nose-up in the gust.

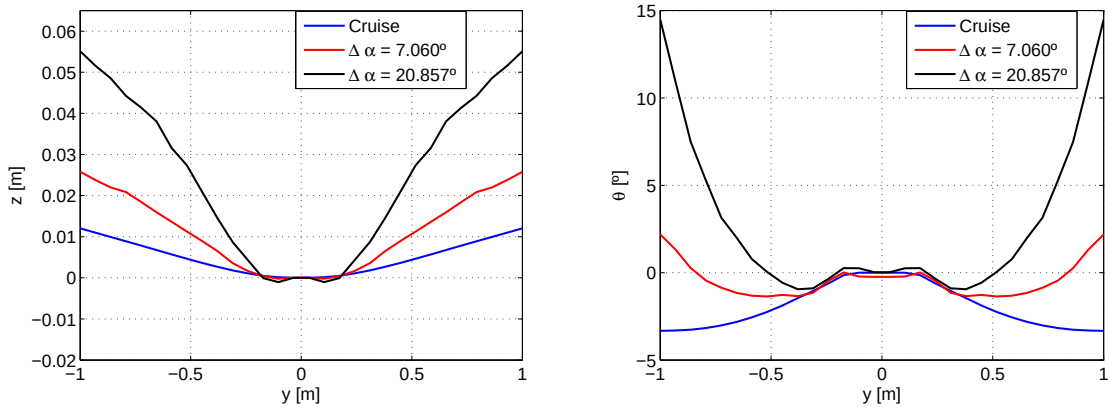

(a) Vertical displacement along the span

(b) Twist along the span

Figure 5.8: Elastic deformation of the wing with vertical gust

Figure 5.8(a) shows a similar trend and magnitude of the wing bending when encountering a gust for this design and with the standard model. Furthermore, the twist of the wing (figure 5.8(b)) shows an increasing pattern that turns the nose-down twist present at cruise into nose-up twist when entering into the vertical gust, except for the sections of the wing next to the engines, which exert a pitch-down moment on the elastic axis. As explained before, the nose-up twist increases the effective angle of incidence which, in turn, rises the aerodynamic loads.

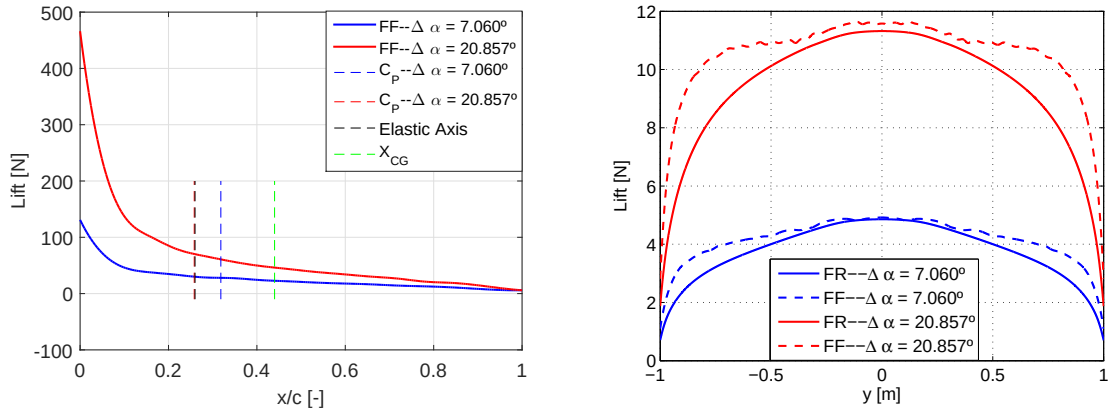

(a) Lift distribution over the chord

(b) Lift distribution over the span

Figure 5.9: Lift distribution over the wing with vertical gust

Looking at the total lift distribution along the chord plotted in figure 5.9(a), we realize that the center of pressure moves towards the quarter-chord line as the angle of incidence increases, being this closer to the elastic axis for the two gust profiles studied. In the case of the least demanding gust profile ($\Delta\alpha = 7.060°$), only the outer part of the wing has a

nose-up twist since the center of pressure remains more rearwards than the elastic axis but closer to it than in cruise conditions. On the other hand, the mean position of the center of pressure for the largest gust profile coincides with the elastic axis, giving as result that the pitch-up torsion is generated mainly by the weight of the wing times the corresponding load factor. Figure 5.9(b) illustrates that the total lift along the span increases, appearing such increment in the outer parts of the wing (sections at which the effective angle of attack is greater). The rise on the loads outwards of the wing increase the bending moment and shear stress at the root, opposite to cruise.

5.3 Structural Modified Design

In previous section it was shown that, although using a cambered airfoil for cruise alleviated the bending moments at the root, when it comes to loads due to vertical gusts, the center of pressure allocates again in front of the elastic axis so there is no alleviation of the load factor, neither reduction stresses at the root for those conditions.

As the center of pressure varies its location with the angle of attack, the previous aerodynamic modification is not appropiate to achieve load alleviation with vertical gust conditions. Due to this reason, the next option is to move the elastic axis whose position depends exclusively on the structure of the wing, it does not vary with the angle of attack. The elastic axis is moved by locating the spar at the leading edge of the wing, placing the elastic axis at 3% of the chord, while being the center of pressure, approximately, at 24% of the chord. In turn, the center of mass is moved to 36% of the chord.

5.3.1 Cruise Analysis

Angles at cruise are obtained as it was done on the previous cases. These are included in table 5.5:

Cruise Results	$\alpha_{\mathbf{wing}} = [^\circ]$	$\alpha_{\mathbf{HTP}} = [^\circ]$
Rigid Structure	2.2803	6.5913
Flexible Structure	2.8696	6.2938

Table 5.5: Cruise analysis for the structural modified design

Moving the spar to the leading has a similar effect than using a cambered airfoil: the angle of attack during cruise for the flexible wing is larger than the one for rigid wing. Moreover, it has an additional effect, the center of mass of the wing is moved forward, reducing the pitch-up torsion produced by it. Nevertheless, the angle of the HTP remains equal than the standard design since the HTP is identical.

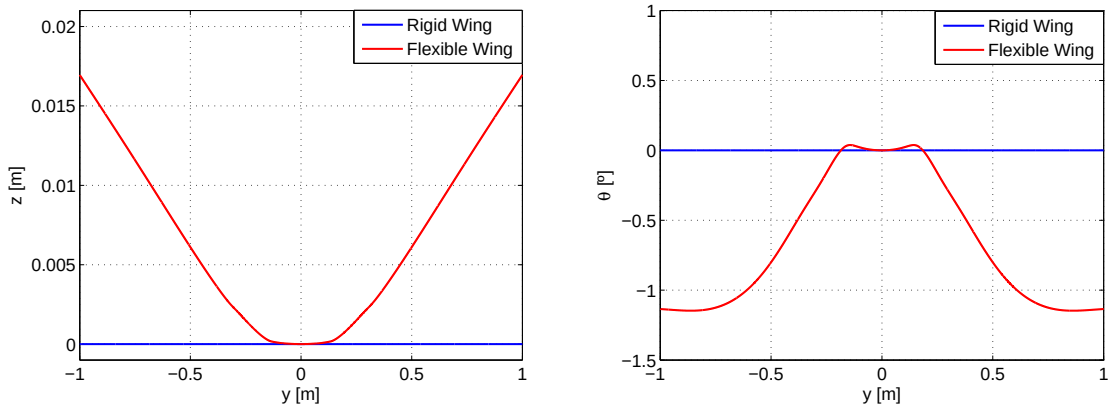

(a) Vertical displacement along the span

(b) Twist along the span

Figure 5.10: Elastic deformation of the wing at cruise

Figure 5.10(a) proves that wing bending behaves as in the other wing configurations. Concerning the twist along the span shown in figure 5.10(b), it is clear that the trend is quite similar to the one of the aerodynamic modified design, the twist is nose-down for cruise conditions, giving rise to a greater angle of attack for the flexible wing compared to the rigid one.

Nevertheless, two main differences can be pointed out by comparison of both cases. The first one is that the elastic twist produced is up to 3 times larger for the aerodynamic modified design than for the structural modified design. This difference is based on the position of the principal wing locations studied. In spite of the fact that the weight of the wing (plus spar) is lower than the lift generated, in this case the center of gravity is further from the elastic axis than the center of pressure, giving as result a lower pitch-down torsion of the wing. The other aspect worth mentioning is that the region next to the fuselage has nose-up twist. The nose-up twist is produced because at that region is where the wing joints attach the wing to the fuselage, increasing the stiffness and moving rearwards the elastic axis. As more rearwards is the shear center, the weight of the wing has a greater contribution to torsion if compared with the moment generated by lift.

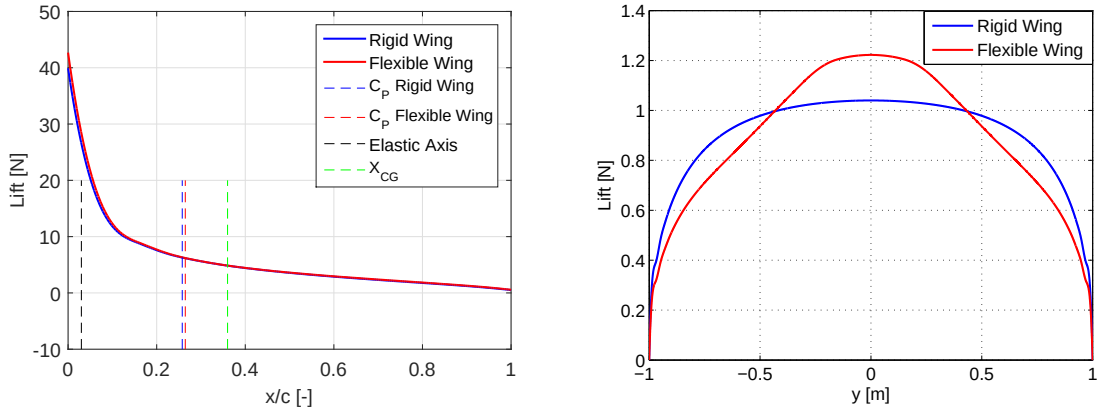

(a) Lift distribution over the chord

(b) Lift distribution over the span

Figure 5.11: Lift distribution over the wing at cruise

Figure 5.11(a) demonstrates that moving the elastic axis forward has the effect of leaving the center of pressure after it, which induces a pitch-down torsion. Nevertheless, the center of mass is also after the elastic axis, counteracting the effect of the lift on the torsion, but not being enough to impose positive twist of the wing at cruise. On the other side, the lift distribution along the span (figure 5.11(b)) follows a similar trend that the aerodynamic modified design, although in this case such lift distribution is close to match the rigid wing lift distribution. This is because the twist produced is not as large as the one of the aerodynamic modified design.

5.3.2 Vertical Gust Analysis

Previously, in the aerodynamic modified design, moving the center of pressure did not result on the desired effect when encountering a vertical gust because the center of pressure moves torwards the quarter-chord line as a function of the angle of attack. By applying the mentioned structural modification, it is intended that, as the center of pressure is already near the quarter-chord line in cruise condition, increasing the angle of attack will not affect the location of the principal locations considered, so the nose-down twist will not turn into nose-up; what is more, the twist is expected to become even more negative, having a benefitial effect on the loads produced by vertical gusts.

	$\Delta\alpha = 7.060°$			$\Delta\alpha = 20.857°$		
	RR	FR	FF	RR	FR	FF
ΔL_{wing} $[N]$	278.61	279.48	232.97	798.54	803.94	695.84
ΔL_{HTP} $[N]$	46.00	45.89	47.64	129.09	128.85	131.57
Load factor (N_z)	3.442	3.448	3.107	7.978	8.017	7.224
Load factor alleviation (%)	-	-0.17	9.71	-	-0.49	9.45

Table 5.6: Gust encounter analysis for the aerodynamic modified design

At last, the data contained in table 5.6 verifies that load alleviation can achieved by moving forward the elastic axis. Albeit in real aircrafts having the elastic axis at the 3% of the chord is not a realistic configuration, a 10% of alleviation has been achieved which implies that better performance when encountering a vertical gust can be reached by placing the elastic axis in an intermediate location between 3%-26% of the chord.

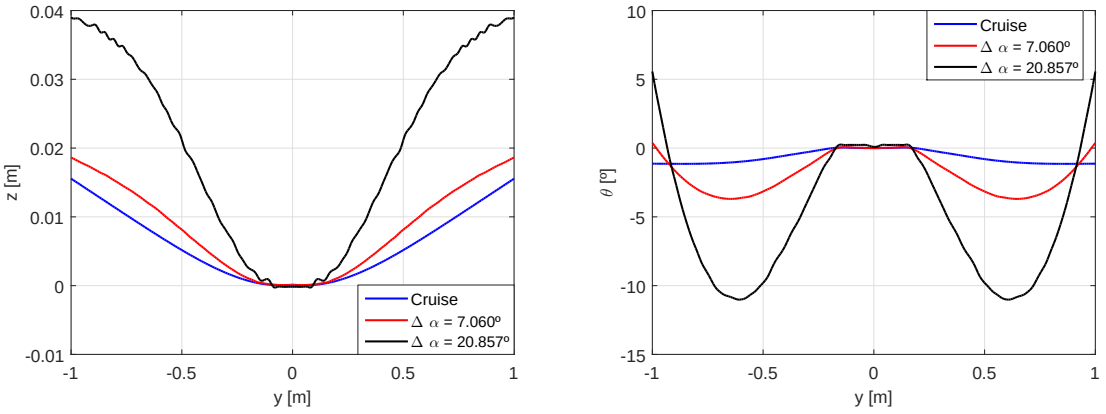

(a) Vertical displacement along the span

(b) Twist along the span

Figure 5.12: Elastic deformation of the wing with vertical gust

Concerning wing bending plotted in figure 5.12(a), it is interesting to remark the small variation of the least demanding gust ($\Delta\alpha = 7.060°$) in contrast to the cruise bending. On the other hand, as figure 5.12(b) shows, there is nose-down twist at most of the wing span, except for a small region at the tips, probably due to the tip vortices that produce a decrease in lift in that section, which makes that the weight-times-load-factor contribution to the torsion is larger that the one related to the lift. However, despite this region, the aim of moving the spar has the net desired effect on the deformations of the wing, a nose-down twist which decreases the effective angle of attack and, thus, the lift generated by a given gust profile. Both deformations are better explained by the lift distribution over the wing.

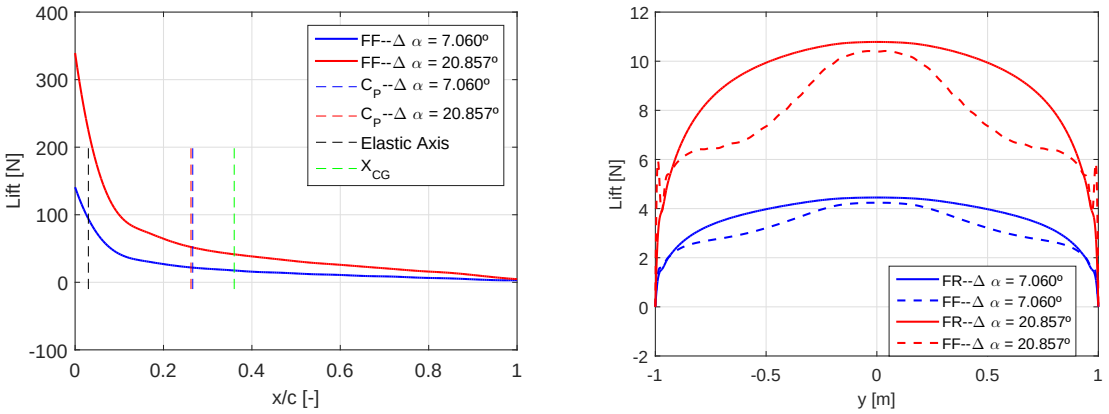

(a) Lift distribution over the chord

(b) Lift distribution over the span

Figure 5.13: Lift distribution over the wing with vertical gust

The main reason why the flexible structure provides load alleviation in comparison with the rigid aircraft is that the center of pressure does not move with the angle of incidence (figure 5.13(a)), which implies that the nose-down twist present in cruise would be maintained even when the angle of attack increases due to the vertical gust. Furthermore, the lift distribution along the span (figure 5.13(b)) shows a discontinuous profile when looking closely to the tips of the wing. At this region there is a step increase in lift. This increase in lift is due to the nose-up twist that is produced on that region, which increases the effective angle of attack and so does the aerodynamic force. In spite of this increase on external force at the tips, the bending moment at the root is still lower than in the rigid case as most of the aerodynamic loads are within the center of the wing. As well, due to the alleviation of the load factor it is implicit the decrease on shear loads and the reduction on the stress at the root of the wing.

As concluding remark of the analysis, a comparison between the different wing configurations is performed. This evaluation is only conducted for the flexible structure as it provides the most accurate data compared with real aircraft performance. The results obtained make clear that locating the elastic axis forward has a huge impact on the load factor. Overlooking the fact that placing the elastic axis next to the leading edge is not a feasible design, a 18% reduction of the load factor (for both gust profiles) has been achieved by moving forward the elastic axis a 23% of the chord. Thus, considering a linear trend, shifting the elastic axis a 1% of the chord forward implies around a 0.8% reduction of the load factor. Hence, a design based on this concept might reduce considerably the loads that the aircraft must withstand.

Chapter 6

Experimental Set-up

One of the objectives of the thesis is to design an experimental procedure to obtain the normal modes of the model and compare them with the ones obtained by means of FEM software. Although there was not enough time during this thesis to perform the test, it is intended to build the specimen and carry out the experimental analysis so the test can be conducted in future works to update the FE model in addition to the aim of using it for teaching purposes in following courses. For these reasons, the specimen that will be tested is designed and the experimental setup required to perform the modal analysis is described.

6.1 Specimen

The best option would be to use as prototype the model that was used to perform the assessment. However, during the study, we realize that it is too large to be handled at the university facilities. For this reason, the previous model is scaled to a smaller specimen which is easier to test. The scaling used is 1:2, meaning that the span of the scaled model will be equal to 1 m. This is applied to the fuselage, wing, engines, HTP & VTP dimensions, except for the thickness that is defined by similarity of modal frequencies with those of the 1:1 model. As well, the spar and the joints are designed based on the natural frequencies of the aircraft.

From the modal analysis and considering the limitations in aluminum processing[1], the 1^{st} wing symmetric bending is not similar to the one of the 1:1 model unless the spar is removed from the design and point masses of 20 gr. are placed at the center of the tips of the wing. The FEM modal analysis for the scaled specimen is the same as the one performed for the original design, taking into account the same assumptions made for that case but recalling the removal of the spar and the attachment of the point masses.

[1]Feasible dimensions and thickness obtained from Alu-Stock catalogue: `http://www.alu-stock.es/`

The modal frequencies of the FE models are contained in table 6.1:

Modes	***Modal Frequencies [Hz]***	
	Original Model	**1:2 Model**
1^{st} symmetric wing bending	7.9675	8.2402
1^{st} VTP bending	9.7681	9.4202
1^{st} asymmetric wing bending	15.804	20.600
1^{st} symmetric wing torsion	17.790	64.118
2^{nd} asymmetric wing bending	19.476	32.255
1^{st} symmetric HTP bending	20.291	25.590
1^{st} VTP torsion	21.614	17.713

Table 6.1: Aircraft aeroelastic modes (Original & 1:2 Scale)

Except for the 1^{st} wing symmetric bending and the 1^{st} VTP bending, none of the other modes has similar frequencies. There are several reasons for this results. The first one, regarding the HTP, similarity has not been achieved due to the limitations inherent to the fabrication of aluminum plates. Secondly, the rest of wing modes do not agree due to the absence of the spar; the wing has been optimized for the 1^{st} wing symmetric bending, not for the rest. Last, and more general, the task of achieving similar modal frequencies is not easy by only scaling a larger model; this implies that, when redesigning the specimen by focusing on one mode it is not certain that the rest of modes will behave similarly. Nevertheless, the disagreement in the modes is not entirely an error since the main objective of the specimen is to update the FEM model, not to present characteristics similar to those of a real aircraft.

The thickness and material for each part that form the prototype are gathered in table 6.2:

Part	**Thickness [mm]**	**Material**
Fuselage	2.0	Aluminium 6063
Wing	2.0	Aluminium 6061
VTP	1.0	Aluminium 6061
HTP	0.8	Aluminium 6061
Engines	1.5	Aluminium 6063
Wing joints	1.5	Aluminium 6063
VTP joints	1.5	Aluminium 6063
HTP joints	1.5	Aluminium 6063

Table 6.2: Thickness & material of the prototype

The draft with the new dimensions of the parts and their relative positions is presented in appendix A.

Although in a GVT the specimen must be an aircraft 'ready to fly', this test is performed to obtain the modes of the structural model and update the FEM until agreement between modes is reached. For this reason, as the actual modes of the aircraft are not necessary, only the structural model designed is tested.

6.2 Support system

The GVT is intended to reproduce with accuracy the normal modes during aircraft operation. In order to achieve this goal, the boundary conditions of the test must simulate free-free conditions that are present when the aircraft is flying. In the introduction several methods where enumerated. From this methods, the bungee cords suspension is implemented in the test. Bungee suspension is the best option because it allows to lower the frequencies of the aircraft rigid body modes [1] and it is the most simple and cheap. The bungee cord suspension system is designed based on the one showed in figure 6.1:

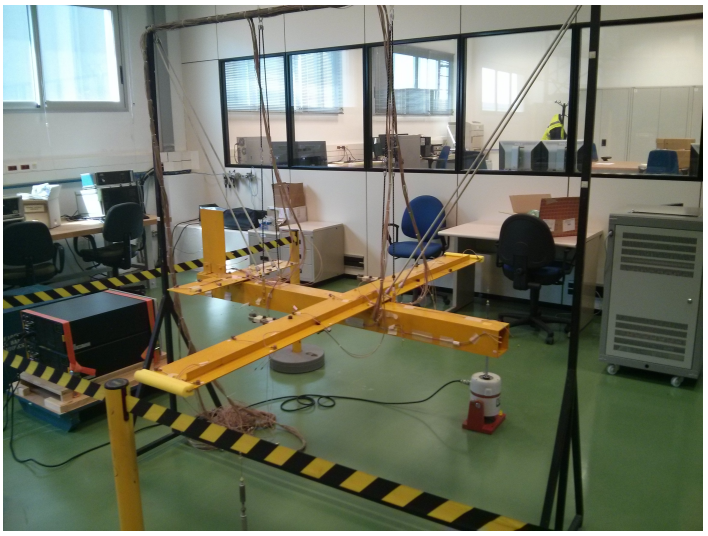

Figure 6.1: Bungee cord suspension system

6.3 Structure Excitation

The model must be excited to obtain the aeroelastic modes of the structure. Some examples of how to excite an aircraft were included in the GVT review presented in chapter 1. From all of them, shakers are the best option and the excitation method that is implemented in the experimental procedure. Two shakers are needed to allow to excite the structure symmetrically and anti-symmetrically. The shakers proposed are SmartShakers^{TM}K2007E01[2] which are electrodynamic exciters.

[2]The Modal Shop: `http://www.modalshop.com/excitation/SmartShaker-with-Integrated-Power-Amplifier?ID=272`

The excitation applied will be a sine sweep. In sine sweep testing one frequency is excited at a time "sweeping" the test frequency range. The sweep speed is relatively slow to ensure good quality (about 0.5 octaves/min). In real aircraft GVT the typical range goes from 0 to 30 Hz., or in some cases 50 Hz., but this range should be adjusted to the particular model under study to ensure that all the modes of interest lay within the analysed range. Sine sweeps are performed using two shakers symmetrically arranged. As well, in order to excite symmetric and antisymmetric modes, two sweeps of phase 0° and 180° are performed [8].

6.4 Data acquisition

The next step is to determine the instrumentation that must be used to obtain the frequencies of the aeroelastic modes. Aircraft vibration response is obtained by accelerometers located along the main parts of the wing.

The selected ones are PCB model 333B30 ICP® 100 mV/g accelerometers. Also, PCB model 208C02 ICP® 11.24 mV/N force cells are located in the shakers in order to obtain the force that is being transmitted to the prototype.

The accelerometers are distributed along the fuselage, wing and HTP as shown in figure 6.2.

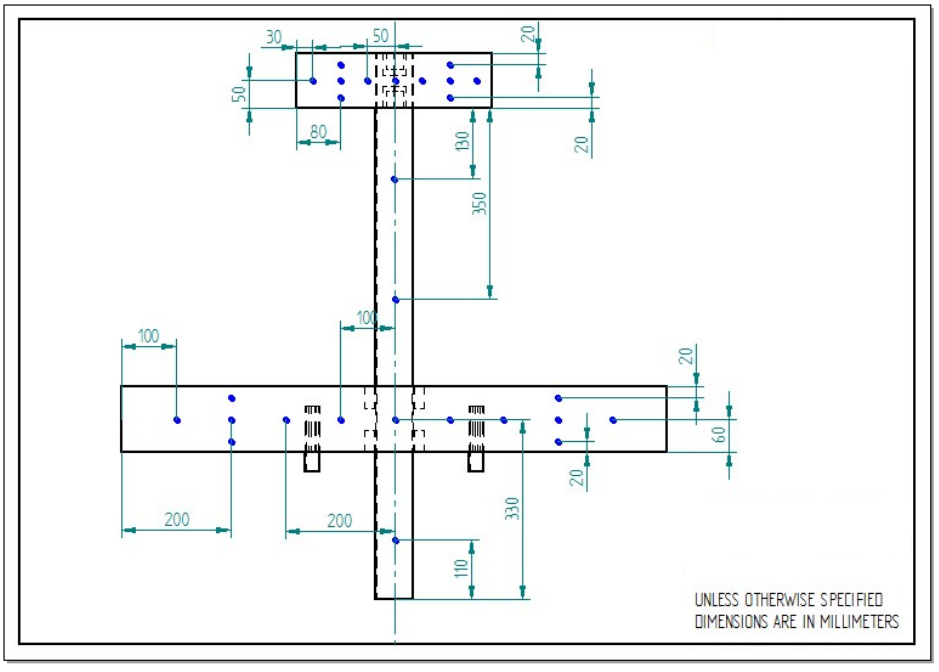

Figure 6.2: Accelerometers distribution

The accelerometers are connected to the data acquisition system, SCADAS mobile, through the V8-E acquisition module, with low-noise coaxial cables model 003C10. The data is processed by using the LMS Test.Lab Academic software.

Chapter 7

Socioeconomic Environment

7.1 Socioeconomic Impact

Aviation industry entails one of the leading industries worldwide. This fact is based on the great impact that this industry has on the world economy and multiculturalism. Regarding the economic aspect, according to IATA [20], air transport industry encompasses up to 63 million jobs (without taking into account military and space industry). It provides fast transport which becomes essential in the worldwide business in which economy is based. What is more, aviation, if it were considered a country, it would be ranked the 21^{st} country in the world in terms of GDP [14]. Concerning the social impact, aviation industry promotes turism and cultural interchange, allows the delivery of humanitarian aid over the world... All these facts make aviation industry indispensable in the actual world and make that it grows constantly each year.

The continuous growth of air passenger traffic generates an intensive investigation about the performance of aircraft. There is a huge competence between airlines as they want to use the best aircraft, so manufacturers must accomplish specific requirements in order to fulfil the conditions imposed by airlines. This leads to a constant investigation in terms of aircraft performance.

Not only manufacturers must design their aircrafts according to airlines requirements, but also they must fulfil some conditions stated by official regulatory agencies. In terms of safety, aircraft must be able to withstand a series of loads in different conditions. These loads are what determine the structural design. On the other hand, regarding environmental impact, there are some limits concerning the CO_2 expelled to the atmosphere. Up to 700 million tons of CO_2 produced in 2015 (2% of human-produced CO_2) and, as aviation industry is constantly growing, some rules and objectives are defined by IATA [19]:

- An improvement on fuel efficiency of 1.5% per year from 2009 to 2020.
- 50% CO_2 reduction from 2005 to 2050.
- Reduce NOx, CO and particulate matter (PM).

Due to the importance of aircraft performance and environmental impact, engineers study the possible designs that allow to achieve the proposed objectives. Within all the possibilities, one of the main options is to reduced the weight of the aircraft. Weight reduction implies a more efficient aircraft which requires less fuel to cover a specific distance. Fuel represents a 28% of the total cost of an airline. Consequently, reducing the weight of the aircraft would have a double impact: lower costs entail a competitive advantage and lower burned fuel help on the aim of reducing the expelling of noxious gases to the atmosphere.

Some of the actual trends on aircraft design are based on using composite materials which provide a high strength to weight ratio, good fatigue strength and corrosion resistance [5]. The expected weight reduction that could be obtained implementing this technology will suppose a great competitive advantage for the manufacturer that is able to adapt the composite to the aircraft structure. Instead using composite materials, in this thesis the decrease of aircraft weight is due to the effect of structural flexibility, which allows to achieve load alleviation and the consequent weight reduction.

The load alleviation during vertical gust encounters (the effect of structural flexibility in other critical conditions might also provide lower stresses) reduces the structural requirements for vertical gust condition and, therefore, the weight would decrease as less reinforcement of the critical parts could be applied. According to the work of [26], the approximate expression that relates load factor alleviation and structural weight is the following:

$$\frac{\Delta W_{struct}}{W_{struct}} = \left(\frac{\Delta N_z}{N_z}\right)^{0.604} \tag{7.1}$$

Nevertheless, the case in which load alleviation is achieved is not realistic because such configuration is not assured to fulfil the structural requirements of static loads, fatigue loads... However, lets consider that, instead of a 10% load alleviation, it is possible to reach a 2% load alleviation by implementing an optimum wing configuration that considers the benefitial effect of structural flexibility. With that assumption and applying the previous expression, the structural weight would decrease a 1.2%. Applying the breguet equation [12] with the data corresponding to C-295 (table 2.1), the fuel efficiency improvement due to structural flexibility is obtained:

$$R = \frac{L}{D}\frac{V_c}{C} ln\left(\frac{W_i}{W_f}\right) \tag{7.2}$$

where R is the range, L/D is the aerodynamic efficiency, V_c is the cruise velocity, C is the specific fuel consumption, W_i is the initial weight and W_f is the final weight. Assuming that all the parameters remain the same when the structural weight of the aircraft is reduced a 1.2%, the final expression that determines the fuel reduction (η) due to structural flexibility is the following:

$$\frac{OEW + PL + FW}{OEW + PL} = \frac{0.988 \cdot OEW + PL + (1 - \eta) \cdot FW}{0.988 \cdot OEW + PL} \tag{7.3}$$

The resultant reduction in fuel weight as a function of the payload is illustrated by figure 7.1:

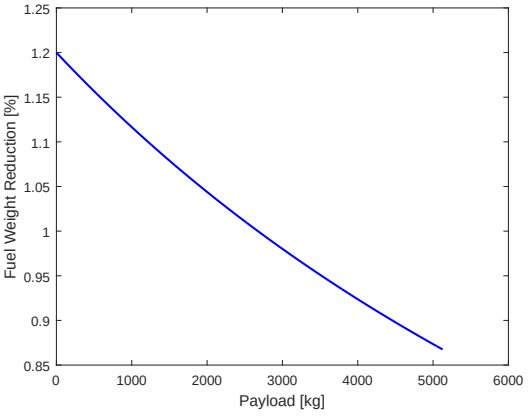

Figure 7.1: Fuel reduction due to OEW decrease

Although it is normal that fuel efficiency is reduced when payload increases, figure 7.1 proves that the potential reduction in structural weight due to flexibility has an important impact on burnt fuel, which, in turn, involves numerous advantages:

- Reduction of airlines operational cost due to the reduction in burned fuel.
- Reduction of noxious gases expelling. IATA objectives in terms of fuel efficiency can be achieved.
- Reducing structural weight allows to increase the payload weight available.
- Lower operational costs for the airlines entail a potential reduction in tickets price, which promotes air transport: encourages globalization, culture interchange, transportation to remote regions, global development...

Despite these advantages concerning the application of this investigation, the experimental setup would have an important social impact as it will be used as part of university courses to help learning about the importance of GVT in certification and the procedures followed to perform this fundamental test.

7.2 Budget

Two different budgets can be associated to this thesis: the one related to the cost of the study itself, and the one related to the manufacturing of the experimental model.

- Cost of the study: it gathers the cost of the licenses of the softwares used to perform the different analyses and procedures, the cost of an engineer working on this investigation and the useful life of the computer used (expected useful life = 5 years).

Details	Quantity	Unit Price (€)	Total Price (€)
Computer	1	800.00	66.67
MATLAB License (Academic)[1]	1	500.00	500.00
ANSYS Mechanical License [2]	1	5000.00	5000.00
Solid Edge License [3]	1	444.00	444.00
1 Engineer	5 months	2000.00	10000.00
Total			16010.67

Table 7.1: Simulation analysis budget

- Experimental Model: it includes all the materials and instruments used to assembly the model and to obtain the modal frequencies.

Details	Quantity	Unit Price (€)	Total Price (€)
Aluminum	-	-	290.22
LMS Test.Lab Academic [4]	15	721.72	10825.80
PCB Model 208C02 [4]	2	435.60	871.20
PCB Model 333B30 [4]	32	346.50	11088.00
Low-noise coaxial cable [4]	32	60.30	1929.60
V8-E Module [4]	1	7782.60	7782.60
SmartShaker^{TM} K2007E01 [4]	2	4230.90	8461.80
Bungee cord suspension system [2]	1	300.00	300.00
Total			41549.22

Table 7.2: Experimental analysis budget

[1] Obtained from: `http://es.mathworks.com/pricing-licensing`
[2] Price estimation
[3] Obtained from: `http://store.plm.automation.siemens.com`
[4] Vibrations analysis system Siemens-LMS: `https://www.plm.automation.siemens.com`

Chapter 8

Conclusion

The main objective of the thesis is to determine the effect of structural flexibility on aircraft loads. For the purpose of achieving this goal, some intermediate tasks were performed. These objectives include:

- Design the FEM model to be analysed.
- Assess the effect of structural flexibility on aerodynamic loads.
- Define an experimental modal analysis set-up that could be used in the future to update the FEM model.

The first task imposed the challenge of designing a structural model equivalent to a real aircraft. Thus, the prototype developed is based on the aeroelastic modal frequencies collected from different sources. Nonetheless, to match all the aeroelastic frequencies for two different aircraft is quite complex as a disagreement in the features that compound the aircraft causes a deviation of some frequencies. For these reason, the aircraft is considered valid when at least three of the frequencies are similar to those obtained from the literature.

Thereupon, the effect of structural flexibility has been evaluated for cruise conditions and in the encounter of an uniform vertical gust. To perform this analysis, a 3D numerical panel method based in vortex ring and horseshoe elements has been developed to compute the aerodynamic loads. ANSYS FEM has been used to obtain the deformations produced by these loads. Then, fluid-structure interaction is implemented to define the complete aeroelastic model. Regarding the conditions at which the study is carried out, these conditions are obtained following different approaches which are currently used for the certification of aircrafts.

The solving process is conducted for three different configurations of the wing to determine which one allows to alleviate the loads in the encounter of a vertical gust. Important conclusions were derived from the analysis:

- The relative position of the elastic axis with regard to the center of pressure and the center of mass of the wing is fundamental in the load factor produced by a vertical gust.
- Although there is some bending of the wing, the elastic twist produced by the aerodynamic loads is the condition that affects mostly to the aerodynamic performance.
- Moving the center of pressure affects to the cruise condition but the increase in angle of attack caused by the vertical gust mitigates its alleviating effect since the center of pressure tends to move back to the quarter-chord line.
- The main option to achieve load alleviation is by moving forward the elastic axis in such a manner that nose-down twist is produced on the wing, thus, decreasing the aerodynamic loads generated for a given angle of attack.

Besides the simulation analysis performed, an experimental model and a GVT procedure are defined. Although it was not possible to carry out the experimental proceeding during the realization of this thesis, the main aspects of this procedure have been set so it can be completed and included in the teaching syllabus of the corresponding university courses.

This paper gives rise to a series of complementary studies concerning this subject. First, once the experimental model is assembled, the experimental procedure included in the thesis should be carried out and the normal modes obtained and compared with the ones calculated with the FEM model. Then, the model should be updated until agreement between experimental and simulation aeroelastic modes is achieved. As mentioned during the thesis, one possible candidate for this mismatch could be found in the model connections, that should be deeply studied. Furthermore, the same analysis could be repeated for several configurations of camber and spar position with the aim of obtaining an approximate trend for these parameters.

Appendix A

Drafts

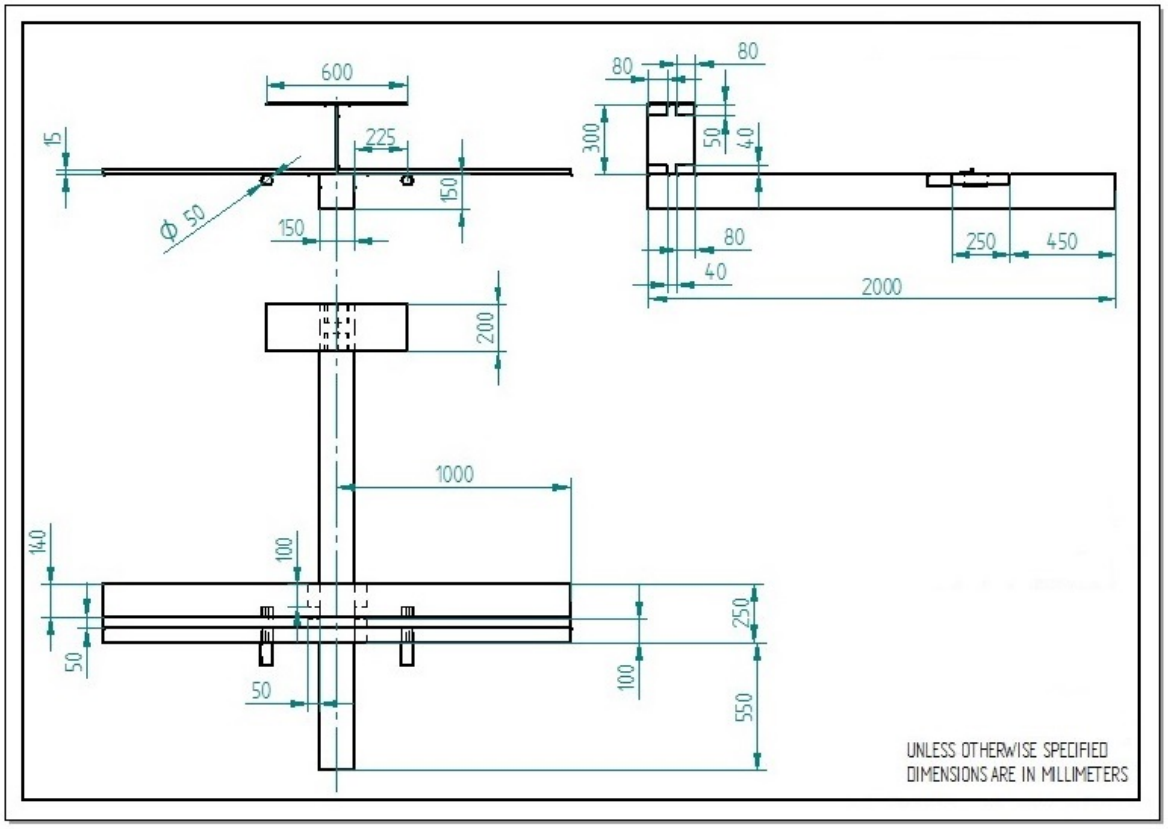

Figure A.1: Original Model

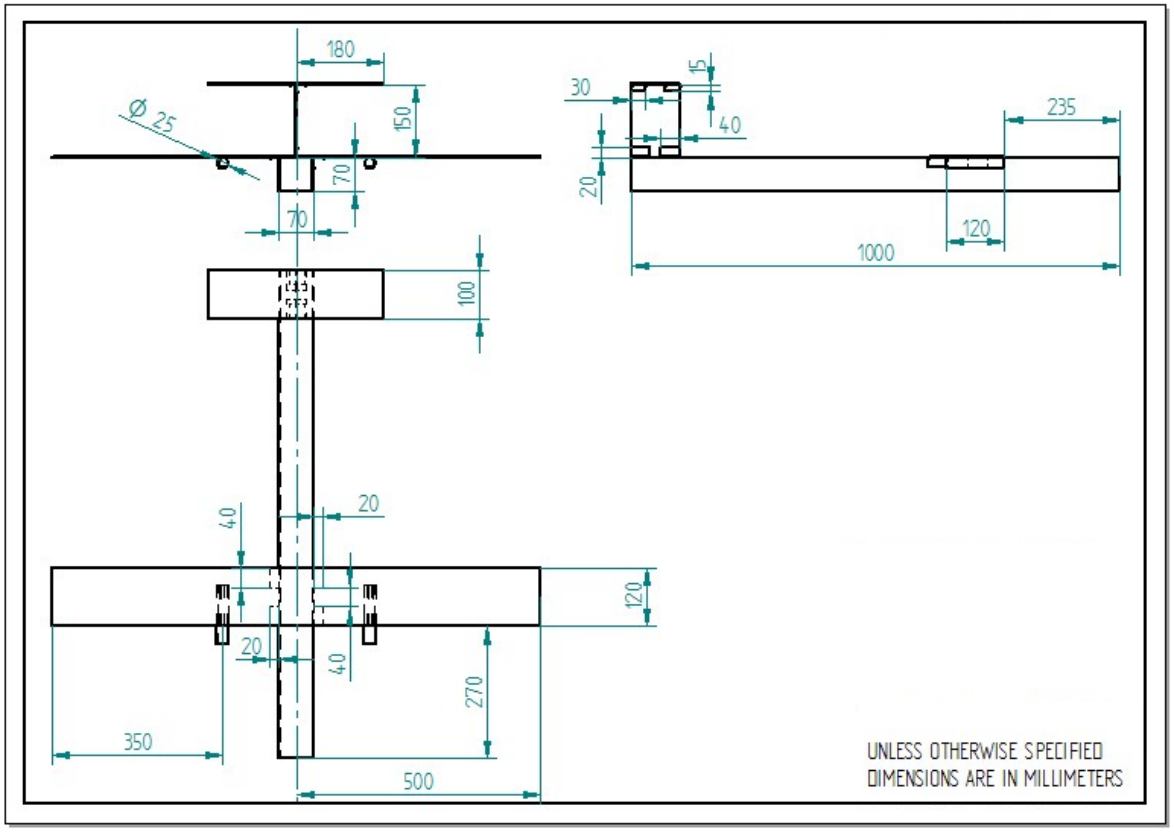

Figure A.2: Scaled Model

Bibliography

[1] Ahlquist, J. R., Carreño, J. M., Climent, H., de Diego, R., & de Alba, J. (2011). Assessment of nonlinear structural response in A400M GVT. In Structural Dynamics, Volume 3 (pp. 1147-1155). Springer New York.

[2] Anderson Jr, J. D. (1985). Fundamentals of aerodynamics. Tata McGraw-Hill Education.

[3] ANSYS v16.2. (2016). ANSYS.

[4] Bisplinghoff, R. L., Ashley, H., & Halfman, R. L. (2013). Aeroelasticity. Courier Corporation.

[5] Botelho, E. C., Silva, R. A., Pardini, L. C., & Rezende, M. C. (2006). A review on the development and properties of continuous fiber/epoxy/aluminum hybrid composites for aircraft structures. Materials Research, 9(3), 247-256.

[6] Bottega, W. J. (2014). Engineering vibrations. CRC Press.

[7] Climent, H. (n.d.). Lecture 2: 2D Aeroelasticity. Universidad Carlos III de Madrid.

[8] Climent, H. (n.d.). Lecture 5: Ground Vibration Test. Universidad Carlos III de Madrid.

[9] Climent, H. (n.d.). Lecture 12: Dynamic Flight Loads. Universidad Carlos III de Madrid.

[10] CS25, E.A.S.A. (2012). Certification specifications and acceptable means of compliance for large aeroplanes. Amendment, 14, 12.

[11] CS-VLA, E.A.S.A. (2003). Certification Specifications for Very Light Aeroplanes. European Aviation., Safety Agency, 18.

[12] Cumpsty, N., & Heyes, A. (2015). Jet propulsion. Cambridge University Press.

[13] EASA.A.186, E.A.S.A. (2011). Type-Certificate Data Sheet EASA.A.186 for CN-235/C-295. European Aviation., Safety Agency, 18.

[14] Economics, O. (2014). Aviation Benefits Beyond Borders.

[15] Federal Aviation Administration. Braniff Airways Flight 542, Lockheed Model L-188A Electra, N9705C; Northwest Airlines Flight 710, Lockheed Model L-188C Electra, N121US. Retrieved from http://lessonslearned.faa.gov/ll_main.cfm?TabID=2&LLID=7&LLTypeID=2. Accessed: 15/04/2016.

[16] Guo, S., Los Monteros, D., Espinosa, J., & Liu, Y. (2015). Gust Alleviation of a Large Aircraft with a Passive Twist Wingtip. Aerospace, 2(2), 135-154.

[17] Heinze, S. (2007). Aeroelastic concepts for flexible aircraft structures.

[18] Iata.org. (2016). IATA - Airlines Continue to Improve Profitability. [online] Available at: http://www.iata.org/pressroom/pr/Pages/2015-12-10-01.aspx [Accessed 15/04/2016].

[19] IATA. (2016). Fact Sheet: Climate Change.

[20] IATA. (2016). Fact Sheet: Economic & Social Benefits of Air Transport.

[21] Jacob, J. D. (2010). Gust encounters in rigid and flexible fixed wing MAVs. Circulation, 900, s2.

[22] Katz, J., & Plotkin, A. (1991). Low-Speed AerodynamicsFrom Wing Theory to Panel Models. Int. edn.

[23] Kerschen, G., Peeters, M., Golinval, J. C., & Stephan, C. (2013). Nonlinear modal analysis of a full-scale aircraft. Journal of Aircraft, 50(5), 1409-1419.

[24] Leissa, A. W. (1969). Vibration of plates. OHIO STATE UNIV COLUMBUS.

[25] Matlab R2012. (2012). Mathworks.

[26] Modlin, C. T., & Zipay, J. J. (2014). The 1.5 & 1.4 Ultimate Factors of Safety for Aircraft & Spacecraft-History, Definition and Applications.

[27] Patil, M. J., & Hodges, D. H. (2004). On the importance of aerodynamic and structural geometrical nonlinearities in aeroelastic behavior of high-aspect-ratio wings. Journal of Fluids and Structures, 19(7), 905-915.

[28] Raghavan, B., & Patil, M. (2007). Aeroelasticity and Flight Dynamics of Oblique Flying Wings. In 48th AIAA/ASME/ASCE/AHS/ASC Structures, Structural Dynamics, and Materials Conference (p. 2240).

[29] Sankar, B. V. (1993). A beam theory for laminated composites and application to torsion problems. Journal of applied mechanics, 60(1), 246-249.

[30] Schweiger, J., & Krammer, J. (2000). Active aeroelastic aircraft and its impact on structure and flight control systems design. DAIMLER CHRYSLER AEROSPACE AG MUENCHEN (GERMANY) MILITARY AIRCRAFT DIV.

[31] Solid Edge V19. (2012). Siemens.

[32] Timoshenko, S. P., & Woinowsky-Krieger, S. (1959). Theory of plates and shells. McGraw-hill.

[33] Ting, E., Nguyen, N., & Trinh, K. (2014). Static Aeroelastic and Longitudinal Trim Model of Flexible Wing Aircraft Using Finite-Element Vortex-Lattice Coupled Solution. AIAA Paper, 837.

[34] Vittala, N. V., Pankaj, A. C., & Venkatasubramanayam, D. V. (2010). Flutter analysis of a composite light trainer aircraft. Journal of Scientific and Industrial Research, 69(2), 113-120.

[35] Wright, J. R., & Cooper, J. E. (2008). Introduction to aircraft aeroelasticity and loads (Vol. 20). John Wiley & Sons.

[36] XFLR5 v6.12 (2016). XFLR5.

[37] Xie, C., Wang, L., Yang, C., & Liu, Y. (2013). Static aeroelastic analysis of very flexible wings based on non-planar vortex lattice method. Chinese Journal of Aeronautics, 26(3), 514-521.